Journal Pre-proof

Chalcone derivatives targeting mitosis: Synthesis, evaluation of antitumor activity and lipophilicity

Patricia Pinto, Carmen Mariana Machado, Joana Moreira, José Diogo P. Almeida, Patrícia M.A. Silva, Ana C. Henriques, José X. Soares, Jorge A.R. Salvador, Carlos Afonso, Madalena Pinto, Hassan Bousbaa, Honorina Cidade

PII: S0223-5234(19)30904-3

DOI: https://doi.org/10.1016/j.ejmech.2019.111752

Reference: EJMECH 111752

To appear in: *European Journal of Medicinal Chemistry*

Received Date: 12 August 2019

Revised Date: 22 September 2019

Accepted Date: 1 October 2019

Please cite this article as: P. Pinto, C.M. Machado, J. Moreira, José.Diogo.P. Almeida, Patrí.M.A. Silva, A.C. Henriques, José.X. Soares, J.A.R. Salvador, C. Afonso, M. Pinto, H. Bousbaa, H. Cidade, Chalcone derivatives targeting mitosis: Synthesis, evaluation of antitumor activity and lipophilicity, *European Journal of Medicinal Chemistry* (2019), doi: https://doi.org/10.1016/j.ejmech.2019.111752.

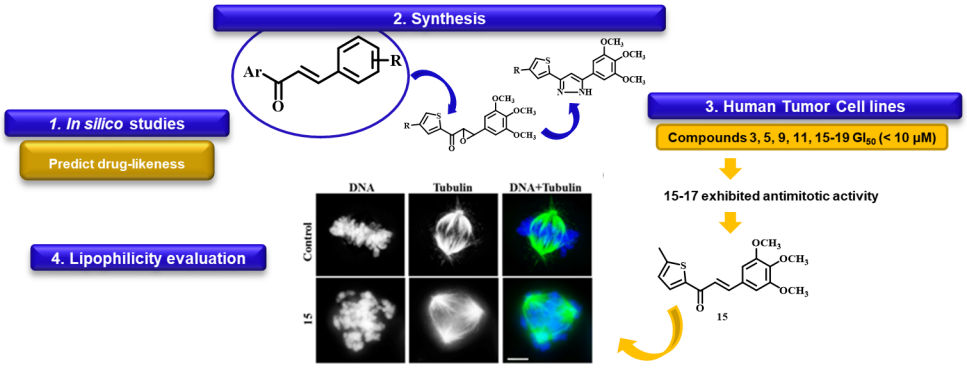

Chalcone derivatives targeting mitosis: synthesis, evaluation of antitumor activity and lipophilicity

Patricia Pinto[a,#], Carmen Mariana Machado[b,#], Joana Moreira[b,c,#], José Diogo P. Almeida[d], Patrícia M. A. Silva[d], Ana C. Henriques[d], José X. Soares[e], Jorge A. R. Salvador[a,f], Carlos Afonso[b,c], Madalena Pinto[b,c], Hassan Bousbaa[d,*], Honorina Cidade[b,c,*]

[a]Laboratório de Química Farmacêutica, Faculdade de Farmácia, Universidade de Coimbra, Pólo III - Polo das Ciências da Saúde, Azinhaga de Santa Comba, 3000-354 Coimbra, Portugal

[b]Laboratório de Química Orgânica e Farmacêutica, Departamento de Ciências Químicas, Faculdade de Farmácia, Universidade do Porto, Rua de Jorge Viterbo Ferreira 228, 4050-313 Porto, Portugal

[c]Centro Interdisciplinar de Investigação Marinha e Ambiental (CIIMAR), Universidade do Porto, Terminal de Cruzeiros do Porto de Leixões, Av. General Norton de Matos s/n 4450-208 Matosinhos, Portugal

[d]CESPU, Instituto de Investigação e Formação Avançada em Ciências e Tecnologias da Saúde (IINFACTS), Rua Central de Gandra 1317, 4585-116 Gandra PRD, Portugal.

[e]LAQV-REQUIMTE, Laboratório de Química Aplicada, Departamento de Ciências Químicas, Faculdade de Farmácia, Universidade do Porto, Rua de Jorge Viterbo Ferreira 228, 4050-313 Porto, Portugal

[f]Centro de Neurociências e Biologia Celular, Coimbra, Portugal.

Abstract

This study describes the synthesis of a series of chalcones, including pyrazole and α,β-epoxide derivatives, and evaluation of their cell growth inhibitory activity in three human tumor cell lines, as well as their lipophilicity using liposomes as a biomimetic

membrane model. Structure-activity and structure-lipophilicity relationships were established for the synthetized chalcones. From this work, nine chalcones (**3**, **5**, **9**, **11**, **15-19**) showing suitable drug-like lipophilicity with potent growth inhibitory activity were identified, being the growth inhibitory effect of compounds **15-17** associated with a pronounced antimitotic effect. Compounds **15-17** affected spindle assembly and, as a consequence, arrested cells at metaphase in NCI-H460 cells, culminating in cell death. Amongst the compounds tested, compound 15 exhibited the highest antimitotic activity as revealed by mitotic index calculation. Moreover, **15** was able to enhance chemosensitivity of tumor cells to low doses of paclitaxel in NCI-H460 cells. The results indicate that **15** exerts its antiproliferative activity by affecting microtubules and causing cell death subsequently to a mitotic arrest, and thus has the potential for antitumor activity.

Keywords: chalcones; antitumor activity; mitosis; lipophilicity; paclitaxel chemosensitivity

[*]**Corresponding authors email addresses:** hassan.bousbaa@iucs.cespu.pt (H. Bousbaa) and hcidade@ff.up.pt (H. Cidade)

[#]Authors contributed equally to this work

1. Introduction

Microtubules are long hollow cylindrical protein polymers made of α- and β-tubulin heterodimers, and, together with actin filaments and intermediate filaments, constitute the major cytoskeletal components in all eukaryotic cells [1]. They have structural roles, such as cell shape and polarity, and dynamic roles such as cell motility, intracellular transport of vesicles and organelles, and chromosome movements in mitosis [1]. Microtubules form the mitotic spindle in charge of delivering chromosomes to the two daughter cells and, hence, the success of mitosis depends on proper microtubule function. Microtubule targeting agents (MTAs), also known as antimitotic drugs, disrupt microtubule function and activate the spindle assembly checkpoint (SAC) in response to defective spindle assembly or spindle□chromosome attachment. As a consequence, cells are chronically arrested in mitosis and eventually die by apoptosis, making microtubules interesting targets for the development of anticancer drugs [2]. MTAs include taxanes and vinca alkaloids which continue to be widely used in the clinic [3]. Taxanes, such as paclitaxel and docetaxel, are microtubule stabilizing agents by promoting tubulin polymerization. Vinca alkaloids, such as vinblastine and vincristine, are microtubule destabilizers by inhibiting microtubule polymerization. However, these MTAs have limited effectiveness in many malignancies due to hematopoietic and neurologic toxicities owing to the role of microtubules in non-tumor cells [3]. Also, their efficacy can be reduced due to drug resistance as a consequence of upregulation of transmembrane efflux pumps that lowers intracellular drug concentrations, and tubulin mutations that affect drug binding sites or alter the expression of different tubulin isotypes [4]. Therefore, the search for new MTAs, that can overcome the disadvantages associated with the MTAs currently in use, continues to be a very active area of research [5].

Chalcones represent one of the major classes of flavonoids that have long been known for their wide range of biological activities, including antitumor activity [6-11]. Moreover, the α,β-unsaturated ketone moiety of chalcones makes these compounds valuable chemical substrates for the synthesis of bioactive derivatives, namely heterocyclic ring systems like pyrazoles [12] . Over the last few years, the discovery of chalcones with antimitotic activity has drawn much attention [13]. Inspired by this, our

research group has reported several chalcones with notable growth inhibitory activity in human tumor cell lines [14-18]. The study of the mechanisms underlying this inhibitory effect resulted in the identification of two chalcone derivatives, **1** and PC2 (**2**), with antimitotic effect (**Figure 1**) [19, 20]. Both chalcones caused abnormal spindle apparatus assembly and a prolonged mitotic arrest followed by cell death [19, 20]. These results support the idea that chalcones **1** and **2** represent a good starting basis for the design of new potential antitumor agents targeting mitosis with improved antitumor properties.

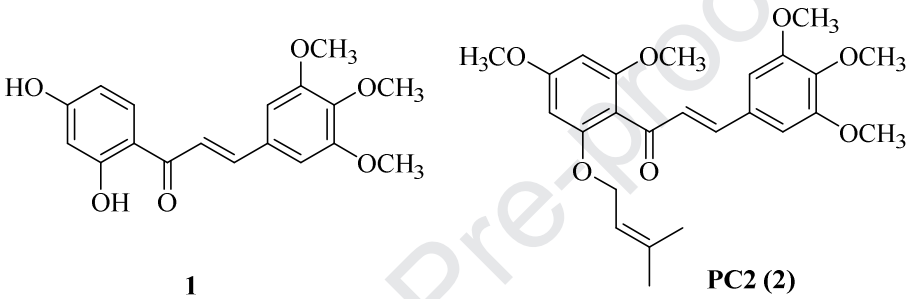

Figure 1. Chemical structure of chalcones **1** and PC2 (**2**).

The action of drug relies on the correct balance between its pharmacokinetic (PK) and pharmacodynamic (PD) behavior. The concept of drug-likeness emerged from the seek for this PK/PD balance [21], being defined by a set of molecular descriptors and/or physicochemical properties which are used to identify the suitable features for a compound to became a drug [22, 23]. Inspired by the pivotal work of Lipinski and his "rule of five", several authors have proposed different set of criteria to evaluate drug-likeness [24-30]. As the majority of molecular descriptors and physicochemical properties can be calculated or predicted by *in silico* methods, its values can be used to roughly evaluate the compound drug-likeness even before its synthesis.

Among the several drug-like features, lipophilicity is one of the most important parameters [31] , namely in the case of taxanes, the most prominent class of MTA agents. In fact, taxanes are very lipophilic agents, exhibiting poor oral bioavailability, and requiring the use of co-solvents which are associated with hypersensitivity reactions

and peripheral neuropathy [32, 33]. Usually, lipophilicity is assessed by measuring the partition coefficient (Log P) drug between water and *n*-octanol [21, 31, 34] . However, the *n*-octanol:water system fails to encode all interactions that occur during drug permeation across biological membranes [35]. In this context, biomimetic models have been gaining increasing relevance as alternative to the classical log P determination because they mimic the duality hydrophobic/hydrophilic environment present in biological membranes [35-37]. Among the different biomimetic models, 1,2-dimyristoyl-sn-glycero-3-phosphorylcholine (DMPC) liposomes are suitable models to assess drug lipophilicity [38].

Hence, in continuation of our efforts to obtain new chalcone derivatives with improved antitumor and antimitotic activity, a small library of chalcones structurally related with **1** and **2**, has been envisioned and preliminary assessed for their drug-likeness properties. These compounds were designed to evaluate the effect of the substitution pattern of A and B phenyl rings in the antitumor and antimitotic activities. The analogues were synthesized and evaluated for their *in vitro* growth inhibitory activity against three human tumor cell lines, A375-C5 (melanoma), MCF-7 (breast adenocarcinoma) and NCI-H460 (non-small cell lung cancer). The antimitotic effect of the chalcones showing potent growth inhibitory effect was characterized. Furthermore, the compounds lipophilicity was determined using liposomes as biomimetic model.

2. Results and Discussion

2.1. Drug-likeness of the chalcones library

Inspired by **1** and PC2 (**2**), a small library of chalcones was designed and *in silico* studies were performed to predict drug-likeness. The drug-likeness was evaluated accordingly to the following chemical features: i) size, inferred by molecular weight (MW); ii) flexibility, inferred by the number of rotatable bonds (RB); iii) unsaturation, inferred by fraction of carbon sp^3 (Fsp^3); iv) solubility, inferred by log S; v) polarity, inferred by polar surface area; and vi) lipophilicity, inferred by the log P. For each designed chalcone, the abovementioned molecular descriptors/physic-chemical properties were calculated (**Table S1 – Table S4 – Supporting materials**). For each chemical feature, the obtained mean values were plotted against the range of values

preconized by the drug-likeness guidelines (**Figure 2a**). Solubility, polarity, lipophilicity, size, and flexibility were within the drug-like chemical space, while unsaturation is the only feature that was not within the preconized limits. However, the high unsaturation degree is a characteristic of the chalcone scaffold and *per si* cannot invalidate the design of this library.

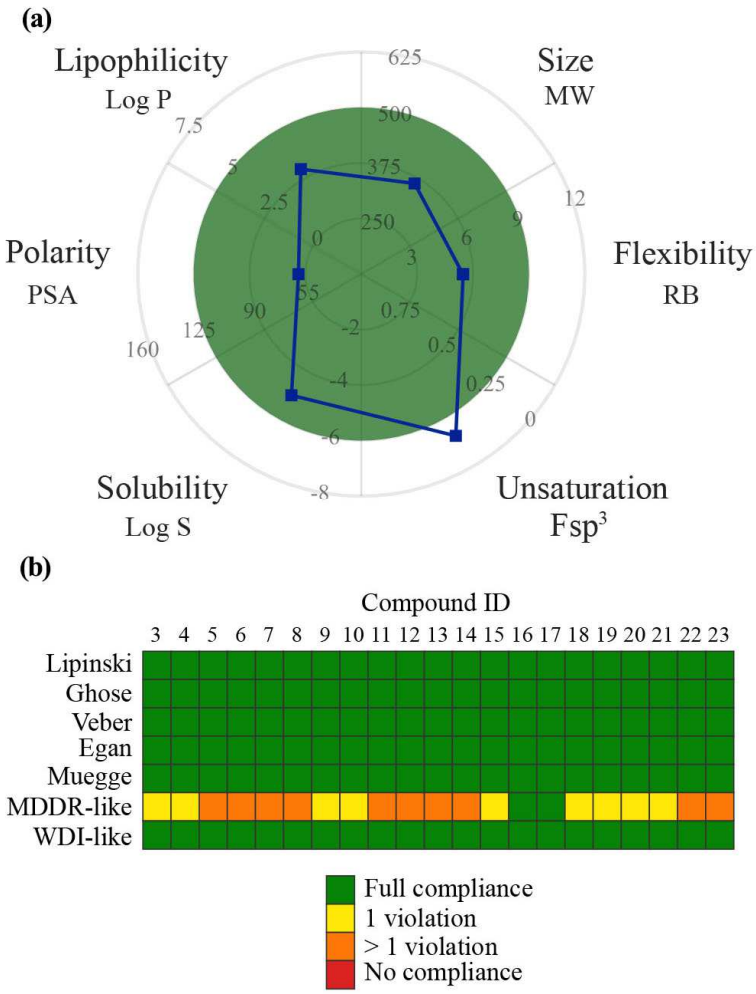

Figure 2. (**a)** Polar plot of the chalcones chemical space. For each feature, mean values were plotted in polar coordinates. Green colored zone represent the range of values preconized for the drug-like chemical space. (**b)** color map of the compliance with the rules of Medicinal Chemistry.

Molecular descriptors and physicochemical properties of the designed chalcones were framed accordingly to the "rules" of medicinal chemistry (**Figure 2b**). The designed compounds fulfill the requirements preconized by different medicinal chemistry "rules",

with the exceptions of the MDDR-like rule. The designed derivatives that violated one criteria of MDDR-like have number of rings < 3, and the ones that violated two criteria have also a number of rotatable bonds < 6. Once again, these features were mostly imposed by the chalcone scaffold.

2.2. Synthesis and tumor cell growth inhibitory activity evaluation

Chalcones **3-23** were synthesized according to the strategy illustrated on **Scheme 1a**. The synthesis of chalcones **3-23** was accomplished through base-catalyzed aldol condensation reactions of appropriately substituted acetophenones and benzaldehydes by microwave (MW) irradiation (**Scheme 1a**). According to the ^{1}H NMR data all chalcones showed *trans* configuration ($J_{H\alpha\text{-}H\beta}$ =15.4-15.7 Hz). ^{13}C NMR assignments were determined by 2D heteronuclear single quantum correlation (HSQC) and heteronuclear multiple bond correlation (HMBC) experiments.

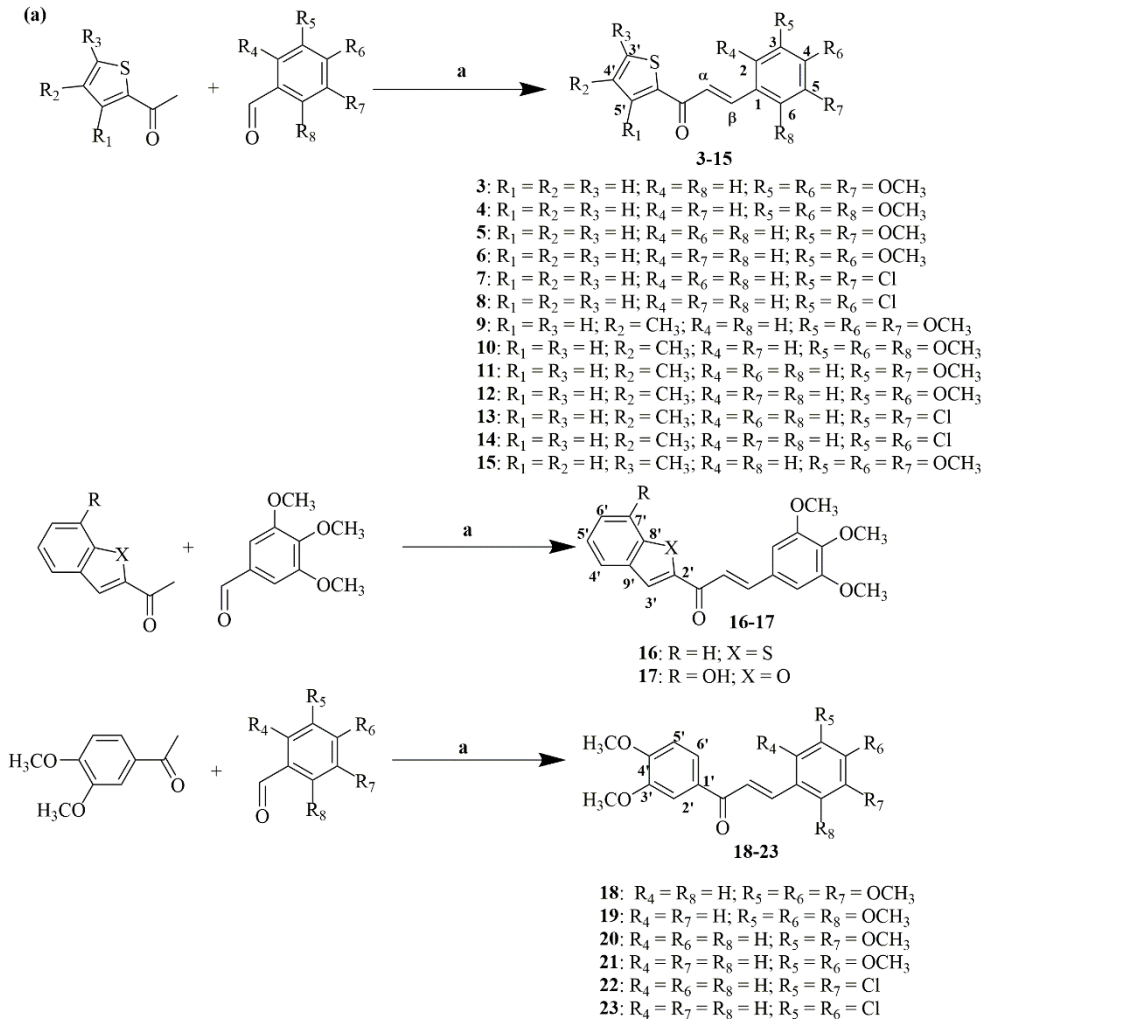

Scheme 1. Synthesis of chalcones. **a)** 40% NaOH/CH_3OH, MW **b)** H_2O_2/5% NaOH, CH_3COCH_3/CH_3OH (3:2), r.t. or H_2O_2/5% K_2CO_3/CH_3OH, r.t.; **c)** Hydrazine hydrate, *p*-toluenesulfonic acid, Xylenes and dichloromethane, 100 ºC, 3-5 h.

The effect of chalcones on the *in vitro* growth of three human tumor cell lines, A375-C5 (melanoma) MCF-7 (breast adenocarcinoma) and NCI-H460 (non-small cell lung cancer) was evaluated according to the procedure adopted by the National Cancer Institute (NCI, USA) which uses the protein-binding dye sulforhodamine B (SRB) to assess cell growth as described in the materials and methods section. A dose response

curve was obtained for each cell line, and the concentration of each tested compound that caused cell growth inhibition of 50% (GI_{50}) was determined.

Table 1. Growth inhibitory effect of compounds **3**-**27** on human tumor cell lines.

	GI_{50} (μM)		
	A375-C5	MCF-7	NCI-H460
3	3.63 ± 0.58	5.95 ± 0.88	5.06 ± 0.20
4	11.12 ± 0.96	12.60 ± 2.68	13.62 ± 2.61
5	4.15 ± 0.85	7.70 ± 2.32	7.12 ± 0.20
6	17.77 ± 5.08	23.92 ± 7.18	17.76 ± 2.97
7	5.38 ± 1.47	11.65 ± 4.57	8.34 ± 2.02
8	7.25 ± 2.97	12.12 ± 2.33	8.44 ± 2.13
9	3.21 ± 0.45	3.26 ± 0.11	3.02 ± 0.01
10	6.96 ± 0.65	10.06 ± 3.70	7.48 ± 0.41
11	3.33 ± 1.18	4.28 ± 2.17	4.44 ± 0.87
12	11.27 ± 1.30	10.78 ± 4.44	15.28 ± 2.85
13	7.14 ± 1.87	12.17 ± 2.79	11.85 ± 3.46
14	12.14 ± 1.87	22.54 ± 1.84	15.50 ± 5.66
15	5.70 ± 1.45	5.56 ± 1.51	6.28 ± 0.31
16	6.90 ± 1.10	6.89 ± 0.41	6.61 ± 0.63
17	8.57 ± 1.06	9.75 ± 1.24	8.35 ± 0.31
18	2.89 ± 0.19	3.97 ± 0.82	5.60 ± 1.20
19	7.10 ± 0.62	8.52 ± 1.03	8.74 ± 1.03
20	3.45 ± 0.54	6.49 ± 0.30	10.84 ± 1.92
21	3.81 ± 0.765	13.15 ± 0.44	8.95 ± 1.01
22	4.51 ± 1.30	8.41 ± 3.63	9.61 ± 2.54
23	4.14 ± 0.70	15.10 ± 0.39	27.68 ± 1.91
24	38.50 ± 4.26	59.92 ± 12.70	61.78 ± 2.04
25	6.63 ± 3.37	14.01 ± 1.73	16.88 ± 3.48
26	> 37.5	> 37.5	> 37.5
27	16.08 ± 2.94	16.34 ± 1.40	16.15 ± 0.56

Results are expressed as GI_{50} (μM) values, tested using A375-C5, MCF-7 and NCI-

H460 cell lines. Doxorubicin (positive control): A375, GI_{50} = 0.014 ± 0.002 µM; MCF-7, GI_{50} = 0.009 ± 0.001 µM; and NCI-H460, $GI_{5}0$ = 0.009 ± 0.002 µM. Data represent mean ± SD of at least three independent experiments performed in duplicate.

As shown in **Table 1**, compounds **3**, **5**, **9**, **11**, **15**-19, and **22** demonstrated the best results of GI_{50} (< 10 µM) in the three human tumor cell lines studied and compounds **7**, **8**, **10**, **13**, **20**, **21**, and **23** also showed promising antiproliferative activity, with a GI_{50} value lower than 10 µM for at least one tumor cell line.

Although the number of compounds is limited, an attempt was made to draw some considerations concerning structure-activity relationship (SAR). Considering the substitution pattern of B ring, some interesting results were observed. Regarding the methoxylated chalcones, when comparing GI_{50} values of 3,4,5-trimethoxychalcones **3**, **9** and **18** with the corresponding 2,4,5-trimethoxychalcones **4**, **10** and **19**, the results revealed that the presence of three methoxy groups on positions 3,4,5 is more favorable for their growth inhibitory activity than the presence on positions 2,4,5. Moreover, the comparison of the GI_{50} values of 3,4-dimethoxychalcones **6**, **12** and **21** with 3,5-dimethoxychalcones **5**, **11** and **20** revealed that the presence of two methoxy groups on positions 3,5 is more favorable than the presence on positions 3,4. These results suggest the importance of 3,4,5-trimethoxyphenyl and 3,5-dimetoxyphenyl B rings for this activity. Regarding the growth inhibitory activity of the chlorinated chalcones, the results showed that the presence of 3,5-dichlorophenyl ring (**7**, **13** and **22**) is more favorable than a 3,4-dichlorophenyl ring (**8**, **14** and **23**) for the studied effect, mainly in A375-C5 and MCF-7 cell lines.

It has been proposed that the presence of conjugated enones in the chalcone scaffold may allow Michael addition of intracellular thiol compounds, such as glutathione, to the olephinic double bond contributing to the enhancement of their antiproliferative activity in human tumor cell lines [39] . Nevertheless, some studies have shown that molecular modification of this enone moiety may led to derivatives with enhanced antiproliferative effect. In fact, for some chalcones the replacement of this moiety by a pyrazole ring has led to chalcone derivatives with improved activity [40] . Therefore, to explore the

impact of modification of the enone moiety on the antiproliferative effect of the two most potent chalcones, **3** and **9**, the pyrazole derivatives **26** and **27** were obtained by molecular modification of **3** and **9**, respectively, according to **scheme 1b**. Firstly, chalcone α,β-epoxide derivatives **24** and **25** were synthesized with 46% and 41% yield, respectively, by the reaction of chalcones **3** and **9** with hydrogen peroxide in the presence of potassium carbonate and methanol. To improve the yields, the epoxidation reaction was then performed using the same oxidant with a stronger basic solution (5% NaOH) in a mixture of acetone:methanol (3:2). Using these conditions both derivatives **24** and **25** were obtained with higher yields (61% and 58%, respectively). After the epoxidation step, pyrazole derivatives **27** and **28** were synthesized by the reaction with hydrazine hydrate in the presence of *p*-toluenesulfonic acid in xylenes and dichloromethane, in very low yields (4-8%).

The antiproliferative activity of these chalcone derivatives on A375-C5, MCF-7, and NCI-H460 cell lines was also evaluated. The comparison of GI_{50} values for the epoxide (**24** and **25**) and pyrazole (**26** and **27**) derivatives with those of corresponding chalcones **3** and **9**, suggests that the substitution of the enone moiety by a three carbon bridge with an epoxide or a pyrazole ring is associated with a decrease in the growth inhibitory effect, particularly for compound **3** (**Table 1**).

2.3. Characterization of the growth inhibitory activity

*2.3.1. NCI-H460 cells arrest in mitosis in response to **15-17** treatment*

Chalcones **3**, **5**, **9**, **11**, **15-19**, and **22** with best results of GI_{50} (< 10 μM) in the three human tumor cell lines were tested for their potential antimitotic effect in NCI-H460 cells. For that, NCI-H460 cells were treated with $3xGI_{50}$ of each compound so as to enhance the potential effect, making antimitotic activity, if any, identifiable within 15 h incubation with the compound. As positive control, cells were treated with 1 μM of nocodazole, a microtubule depolymerizing agent which induces a well-known arrest in mitosis [41]. Phase contrast microscopy examination of treated cells showed an accumulation of bright round-shaped cells, characteristic of mitotic cells, that mirrored that of nocodazole-treated cells, suggesting an antimitotic activity for all compounds tested (**Figure 3a**). DAPI staining of treated cells, to visualize the DNA, confirmed the

presence of an increasing number of cells arrested in mitosis, through observation of condensed chromosomes (**Figure 3a**). In contrast, and as expected, untreated and DMSO-treated cells showed only few cells in mitosis, with the majority of cells at interphase.

We noted that compounds **15-17** exhibited the highest antimitotic activity compared with the other selected compounds tested. This observation was confirmed when we determined the mitotic index (MI) for all the selected compounds, after phase contrast microscopy quantification of mitotic and interphase cells (**Figure 3b**). As expected, untreated cells presented a mitotic index of 11.3%, while nocodazole-treated cells had an increase to 73.1%. All compounds tested induced a significant increase in mitotic index, compared to control treatments. It is noteworthy that cells treated with compounds **15-17** exhibited the strongest antimitotic activity, with a mitotic index between 25.80% and 49.37% (**Figure 3b**). Collectively, these results suggest that compounds **3**, **5**, **9**, **11**, **15-19**, and **22** exert their antiproliferative effect by blocking mitotic progression, being **15-17** the compounds with the strongest antimitotic activity. Interestingly, similarly to the previously identified antimitotic chalcones **1** and PC2 (**2**) [19, 20], and to several MTAs, such as podophylotoxin, combretastatin A4 and colchicine, chalcones **15-17** with the highest mitotic index also possess a 3,4,5-trimethoxyphenyl ring, already described as important for the interaction with tubulin [20]. These results reinforce the importance of a 3,4,5-trimethoxyphenyl ring to obtain compounds with antimitotic effect.

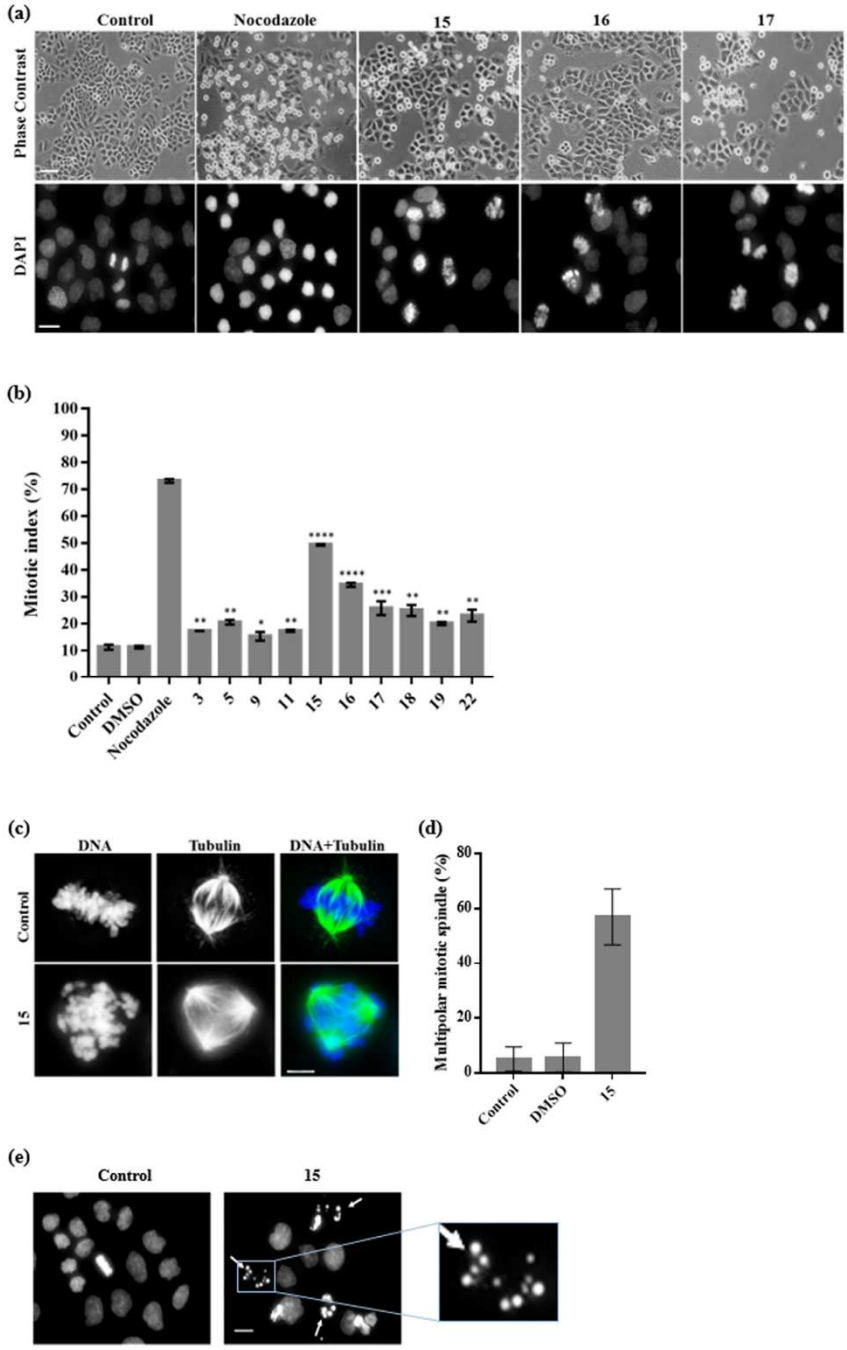

Figure 3. Treatment with **3**, **5**, **9**, **11**, **15-19**, and **22** arrest NCI-H460 cells in mitosis, being this effect associated with alteration in mitotic spindle morphology. (**a**) Representative microscopy fields of mitotic cells (rounded) accumulated in cell culture after 15 h treatment with the indicated compounds, as shown by phase contrast microscopy (upper panel, Bar = 20 μm) and confirmed by DAPI staining of DNA (lower panel, Bar = 5 μm). Similar results were observed with the other compounds.

Nocodazole was used as a positive control. (**b**) Mitotic Index graph showing accumulation of mitotic cells after 15 h of treatment with all selected compounds. Statistical significance of samples treated with the compounds when compared with control, *P<0.05; **P<0.01; ***P<0,001; ****P<0.0001. (**c**) Immunofluorescence staining with anti-α-tubulin antibody. Control metaphase cells exhibited aligned chromosomes (blue) attached to normal microtubule fibers (green) that are assembled into a well-organized bipolar spindle, while **15**-treated cells presented multipolar spindles with misaligned chromosomes. DNA was stained with DAPI (blue). Bar = 5 μm. Similar results were observed with compounds **16** and **17**. (**d**) Mitotic spindles were quantified in control- and **15**-treated cells, the results are expressed as a percentage of multipolar spindles over the total of spindles. Statistical significance of samples treated with **15** when compared with control (*P<0.05). Data represent mean±SD of three independent experiments. (**e**) NCI-H460 cell death was induced upon prolonged exposure to **15**. Extended treatment with compound (24 h) promoted micronucleation and cell death (arrow); the inset shows a fragmented cellular nucleus reminiscent of cell dead by apoptosis. DNA stained with DAPI. Bar = 5μm.

*2.3.2. Mitotic spindle morphology is affected by **15-17***

Chalcones **15-17** with the strongest antimitotic activity were selected for subsequent analysis. Mitotic arrest is often linked to spindle microtubules perturbation, resulting in persistent activation of SAC signaling activation [41] . Accordingly, and since **15-17** treated cells were arrested in mitosis, we then treated NCI-H460 cells with these compounds as above, and performed an immunostaining using an anti-α-tubulin antibody, to visualize the spindle microtubules. DNA was also stained with DAPI. Through fluorescence microscopy observation, we noticed that untreated control cells exhibited microtubule fibers assembled into a well-organized bipolar spindle, while compounds-treated cells showed an abnormal mitotic spindle morphology, mainly consisting of a multipolar spindle (**Figure 3c**). Consistent with microtubule defects, many chromosomes failed to align at the metaphase plate. As the three compounds exhibited similar results, we pursued further analysis with the compound **15** only, because it showed the best antimitotic activity. The morphology of spindles was quantified revealing an increase in multipolar spindles, from 2% of total mitotic

spindles in untreated-cells to 28% in **15**-treated cells (**Figure 3d**). These results suggest that the compounds arrest NCI-H460 cells in mitosis, by interfering with spindle microtubule assembly.

*2.3.3. Assessment of cell fate after prolonged treatment with **15***

In order to characterize the fate of NCI-H460 cells in response to prolonged treatment with **15**, NCI-H460 cells were exposed to **15** treatment for 24 h and stained with DAPI, for DNA evaluation. Through fluorescence microscopy observation, it was verified that cells presented abnormal nuclear morphology, with micronucleation, suggesting cell death (**Figure 3e**). This observed morphology is reminiscent of cells dying by apoptosis, probably as a consequence of prolonged mitotic cell arrest or cell division failure. Further analyses are needed to confirm if the **15**-induced cell death is apoptosis.

*2.3.4. Treatment with **15** sensitizes tumor cells to low nanomolar doses of paclitaxel*

Given its antimitotic activity, we wondered if **15** could enhance chemosensitivity and efficacy of tumor cells to paclitaxel, an antimitotic agent currently used in cancer therapy. The rational is that the two agents should target different aspects of the mitotic spindle, and consequently should mutually increase their efficacy in terms of antimitotic activity and cytotoxicity. Therefore, we performed an MTT viability assay using a combination of **15** compound (at 1x and 0.5xGI_{50} concentrations) and paclitaxel at doses ranging from 2 to 25 nM, for 48 h. As shown in **Figure 4**, concentrations of paclitaxel lower than 25 nM had no significant effect on cell viability. Of note, we found that at 1xGI_{50} **15** was able to sensitize cancer cells to doses as low as 1 nM of paclitaxel, as judged by the resulting decrease in cell viability (46.8%) comparatively to cell viability in the **15** (67.9%) or paclitaxel (92.3%) individual treatments (**Figure 4**). Interestingly, while cell viability was not significantly affected (96.9%) with 0.5xGI_{50} concentration of **15**, its combination with paclitaxel from 5 nM doses greatly compromised cell viability (51.8%). Collectively, these observations suggest that the compound **15** increases the cytotoxic effect of paclitaxel, and that the doses of both antimitotic agents could be lowered in a combination therapy, thereby providing an opportunity to minimize resistance or side effects issues.

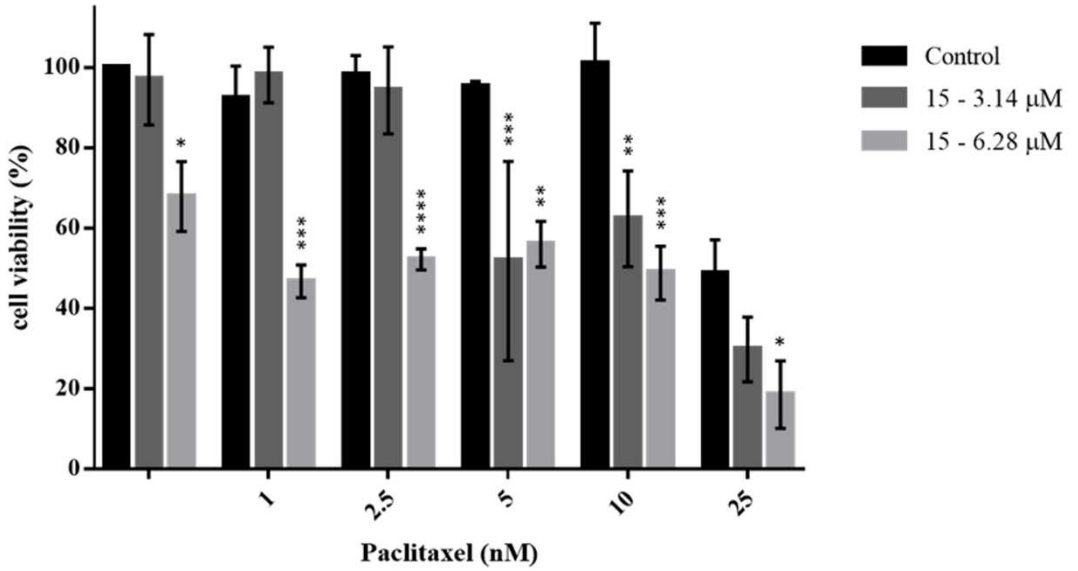

316

317 **Figure 4.** The chalcone **15** enhances sensitivity of cancer cells to paclitaxel. Relative
318 cell viability of NCI-H460 cells treated with **15** (at $0.5xGI_{50}$ or $1xGI_{50}$) in combination
319 with paclitaxel at the indicated concentrations for 48 h. Statistical significance of treated
320 samples when compared with control, *P<0.05; **P<0.01; ***P<0.001; ****P<0.0001.
321 Results are expressed as mean ± SD, from at least three independent experiments.

322 *2.4. Lipophilicity Evaluation*

323 Lipophilicity was evaluated using the gold standard octanol:water system (log P) and
324 the biomimetic system composed by liposomes and buffer at physiological conditions
325 (pH 7.4 and 37 °C). For each compound, log P values were predicted by different *in*
326 *silico* methods (**Table S4 – Support materials**). As depicted in **Figure 5a**, the log P
327 values varied significantly, with standard deviation up to 1 logarithm unit, depending on
328 the *in silico* method used for the prediction. It should be highlighted that compound
329 were identified in pair-wise positional isomers, with exceptions of compounds **13**, **14**,
330 and **15**. Positional isomers had equal predicted log P values (for instance, compound **3**
331 and **4**). This is attributed to the fact that the contributions of each atom/fragment for log
332 P calculation is independent of the atom/fragment position.

333 Partition coefficients in biomimetic models (log K_p) were determined using 1,2-
334 dimyristoyl-sn-glycero-3-phosphorylcholine (DMPC) liposomes as it is a suitable

335 model for this class of compounds [38] . Log K_p were determined by recording its
336 second-derivative absorption spectra in the presence of increasing lipid concentrations
337 at physiological conditions (pH 7.4 and 37 °C) [36] . The experimental data, second
338 derivative *vs.* lipid concentration, at the absorption maximum wavelength is then fitted
339 into Equation 1 to calculate K_p value [42-44] . As an example, **Figure 5b** shows the
340 plot of the second derivative *vs.* lipid concentration at 334 nm for chalcone **17** and its
341 corresponding best fitted curve.

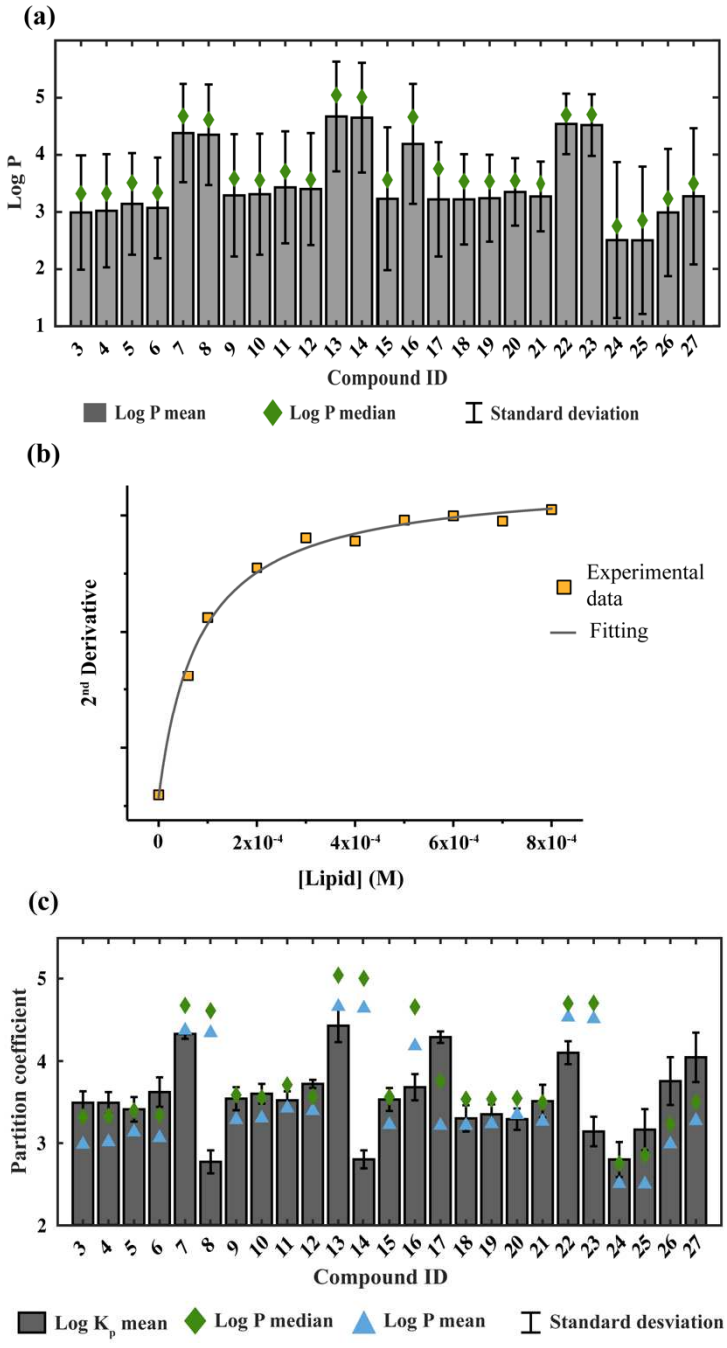

342

Figure 5. (a) Mean, median and standard deviation of the Log P predicted by different *in silico* methods. **(b)** Chalcone **17** best fitting curve to the experimental second-derivative data at a wavelength of 334 nm. **(c)** Experimentally obtained Log K_p values, and mean and median of predicted log P for the studied chalcones.

The experimentally determined log K_p values are in **Table S5 – Support materials**, and summarized in **Figure 5c**. The majority of chalcones showed log K_p values which were slightly higher than the predicted log P values. All compounds were not ionized at pH 7.4, the difference between log K_p and log P relied on the non-aqueous phase. As liposomes are able to take into account more interactions, namely the electrostatic ones, the partition coefficient values obtained with this system were slightly higher. Exceptions to this general trend were the benzothiophene based chalcone **16**, with a log K_P smaller than the log P; the benzofuran based chalcone **17**, with log K_P substantial higher than the predicted log P; and the di-*ortho* chloro-substituted analogues **8**, **14**, and **23**, with log K_P substantial lower than the predicted log P. The behavior verified for chalcone **17** was in accordance with previous reports for very lipophilic compounds (log P around 5) and compounds bearing phenol groups [38] . Regarding the dichlorobenzene based analogues, which had similar predicted log P values, different log K_p values were obtained depending on the position of chloro groups.

From the obtained results, a structure-property relationship (SPR) can be proposed (**Figure 6a**). Concerning the A ring, 1,2-dimetoxybenzene based chalcones had slight lower log Kp values when compared with thiophene based chalcones. For the thiophene based chalcones, the substitution with a methyl group, independently of position, promotes a very slight increase of the log K_P value. Moreover, the substitution of the thiophene moiety for a benzothiophene also promotes a small increase of the log K_P, whereas the substitution for a 7-hydroxybenzofuran promotes a huge increase of the log K_P. When the chalcone enone moiety is substituted by the α,β-epoxide moiety, lipophilicity is decreased, whereas the substitution by a pyrazole moiety lead to an lipophilicity increment. Regarding the B ring, while di-*ortho* chloro-substituted analogues showed log K_P values lower than di-*meta* substituted analogues, di-*ortho* methoxy-substituted analogues showed log K_P values slightly higher than di-meta substituted analogues. This feature is more prominent with di-*ortho* chloro-substituted

analogues. For instance, log K_P of the di-*meta* chlorochalcone **13** was 4.43, and log K_P of the di-*ortho* chlorochalcone **14** was 2.80.

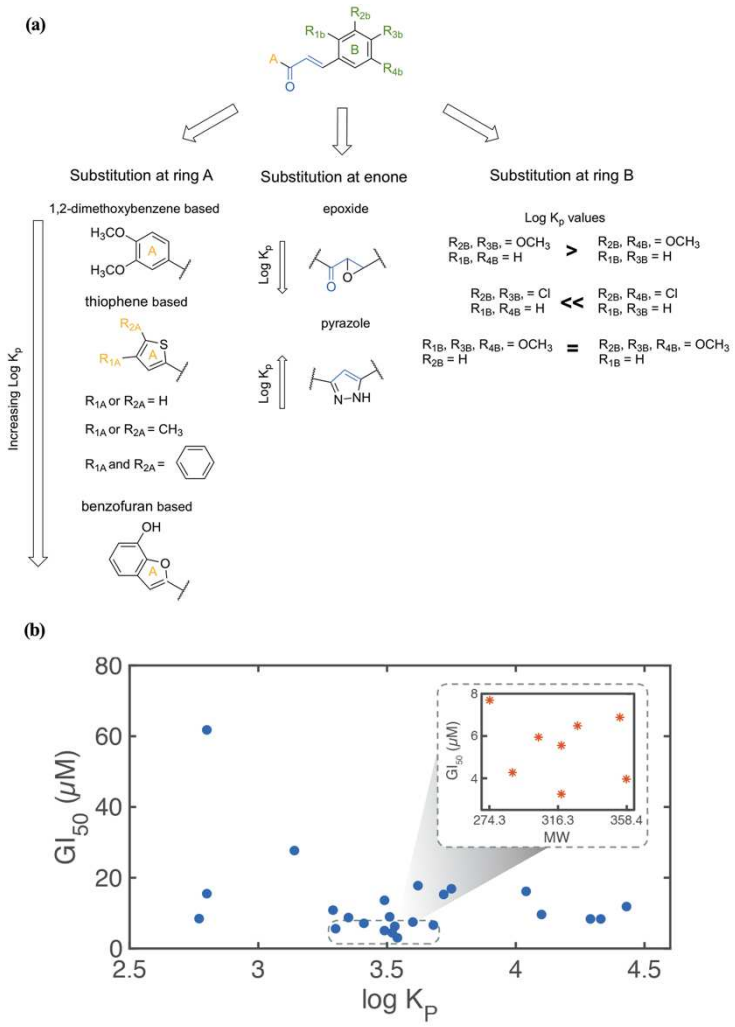

Figure 6. **(a)** Structure-lipophilicity relationship of chalcone derivatives. **(b)** Comparison between the GI_{50} of the chalcone derivatives on NCI-H460 cell line and the log K_P. The insert displays the comparison of the most potent compounds (GI_{50} < 8 μM) and their molecular weight.

GI_{50} and log K_P of the compounds were examined in order to investigate relationship between the compounds lipophilicity and the antiproliferative activity. **Figure 6b** depicts the relationship between lipophilicity and the antiproliferative activity on NCI-H460 cell line. Similar relationships were found on the other cell lines (**Figure S1 – Support materials).** None of the compounds showing a log K_P below 3 exhibited GI_{50} values lower than 10 μM. The most potent compounds (GI_{50} < 8 μM) have log Kp

values between 3.30-3.68 (dashed box, **Figure 6b**). Interestingly, these compounds, that share similar lipophilicity behavior, do not share the same chemical features, as it can been inferred by broad distribution of their molecular weight (as illustrated in the insert of **Figure 6b**). In fact, these compounds have the broadest distribution of size as 274.3 and 358.4 corresponds to the lowest and highest molecular weight of all synthetized compounds, respectively. Moreover, increasing the lipophilicity above 4 did not improve significantly the activity.

3. Material and Methods

3.1. General information

Microwave reactions were performed using a glassware setup for atmospheric-pressure reactions or a 100 mL Teflon reactor (internal reaction temperature measurements with a fiber-optic probe sensor), using an Ethos MicroSYNTH 1600 Microwave Labstation from Milestone. All reactions were monitored by thin-layer chromatography (TLC). The purification of compounds by flash chromatography and preparative TLC was performed using Macherey-Nagel silica gel 60 (0.04-0.063 mm) and Macherey-Nagel silica gel 60 (GF254) plates, respectively. Melting Points were obtained in a Köfler microscope and are uncorrected. Optical rotation measurements were carried out on a Polartronic Universal polarimeter (ADP 410 polarimeter). ^{1}H and ^{13}C NMR spectra were taken in $CDCl_3$ at room temperature, on Bruker Avance 300 and 500 instruments (300.13 MHz or 500 MHz for ^{1}H and 75.47 or 120 MHz for ^{13}C). Chemical shifts are expressed in δ (ppm) values relative to tetrametylsilane (TMS) used as an internal reference; ^{13}C NMR assignments were made by 2D (HSQC and HMBC) NMR experiments (long-range ^{13}C-^{1}H coupling constants were optimized to 7 Hz). The spectral treatment was executed using the MestReNova v6.0.2-5475 software. HRMS mass spectra of compounds **3-23** were performed on an APEXQe FT-ICR MS (Bruker Daltonics, Billerica, MA), equipped with a 7T actively shielded magnet, at C.A.C.T.I.-University of Vigo, Spain. Ions were generated using a Combi MALDI-electrospray ionization (ESI) source. HRMS mass spectra of compounds **24**-**27** were performed on an LTQ OrbitrapTM XL hybrid mass spectrometer (Thermo Fischer Scientific, Bremen, Germany) controlled by LTQ Tune Plus 2.5.5 and Xcalibur 2.1.0. at CEMUP-

University of Porto, Portugal. 1,2-Dimyristoyl-sn-glycero-3-phosphorylcholine (DMPC) was purchased from Avanti Polar Lipids, Inc. (Alabaster, AL, USA). The remaining commercially available reagents were purchased from Sigma Aldrich (St. Louis, MO, USA) and Alfa Aesar (Ward Hill, MA, USA). HEPES buffer (HEPES: 10 mmol L–1, pH 7.4) was prepared using double deionized water from Arium® water purification system (resistivity > 18 MΩ cm, Sartorius, Goettingen, Germany), and the ionic strength was adjusted with NaCl (I=0.1 M). Absorption spectra for log K_P determination were recorded with a microplate reader (Synergy HT; Bio-Tek Instruments, Winooski, VT, USA) and the double beam spectrophotometer (Cary 1E, Varian Inc., Palo Alto, CA, USA) was a JASCO V660. Log S was predicted by 6 programs/online servers, including SwissADME [45], PreADMET [46] , pkCSM [47] , AquaSol [48] , and ALOGPs [49] . PSA was calculated by ChemDraw (v. 18.1), SwissADME [45], and Molinspiration [50]. Log P calculations were given by 6 programs/online servers, including ChemDraw (v. 18.1), SwissADME [45], PreADMET [46], pkCSM [47] , Molinspiration [50], and ALOGPs [49] .

3.2. Synthesis

*Synthesis of chalcones **3-23***. To a solution of appropriately substituted ketone (1.01 - 7.93 mmol, 0.19 - 1.05 g) in methanol (25 mL) was added an aqueous solution of 40% sodium hydroxide (methanol/water) until pH 13 - 14, under stirring and on ice. Then, a solution of appropriately substituted benzaldehyde (2.03 - 15.86 mmol, 0.28 - 3.11 g) in methanol was slowly added to the reaction mixture. The reaction was submitted to successive 15 min periods of microwave irradiation of 180 W of power, with the final temperature of 69 °C. Total irradiation time 2 h - 3 h, and was monitored by TLC. Upon completion, the reaction mixture was poured into ice and the pH was adjusted to approximately 7 with diluted hydrochloride acid. For all chalcones, except **4**, **10**, **12**, **19** and **20** the resulting residue was filtered, washed with water, and purified as described below. For chalcones **4**, **11**, **12**, **19** and **20** the resulting residue was taken in chloroform and further rinsed with water, dried over anhydrous sodium sulfate, evaporated under reduced pressure and the obtained residue was purified as described below.

The structure elucidation of compounds **3**-**6**, **8**, **11**, **1**2, and **18**-**23** was established by ^{1}H and ^{13}C NMR techniques and data were in accordance to the previously reported [51-62]. The structure elucidation of new compounds **7**, **9**-**10**, **13**-**17**, and **24**-**27** was established on basis of HRMS and NMR techniques.

*(E)-3-(3,5-dichlorophenyl)-1-(thiophen-2-yl)prop-2-en-1-one (**7**).* Purified by crystallization (methanol: chloroform). Yield: 46%; mp: 101-103 ºC; ^{1}H NMR ($CDCl_3$ 300.13 MHz): δ 7.89 (1H, dd, J=3.8, 1.1 Hz, H-5'), 7.73 (1H, dd, J=4.5, 1.1 Hz, H-3'), 7.70 (1H, d, J=15.6 Hz, H-β), 7.50 (1H, d, J=1.8 Hz, H-6), 7.41 (1H, d, J=15.6 Hz, H-α), 7.40 (1H, t, J=1.8 Hz, H-4), 7.21 (1H, dd, J=4.9, 3.9 Hz, H-4'), 6.50 (1H, d, J=1.8 Hz, H-2,-6); ^{13}C NMR ($CDCl_3$, 75.47 MHz): δ 181.3 (C=O), 145.1 (C-2'), 140.9 (C-β), 137.7 (C-3,-5), 135.7 (C-1), 134.6 (C-3'), 132.3 (C-5'), 130.1 (C-4), 128.4 (C-4'), 126.5 (C-2,-6), 124.0 (C-α); ESI-HRMS (+) *m/z*: Anal. Calc. for $C_{13}H_9Cl_2OS$ $(M+H)^+$: 282.97457; found: 282.97482.

*(E)-1-(4-methylthiophen-2-yl)-3-(3,4,5-trimethoxyphenyl)prop-2-en-1-one (**9**).* Purified by crystallization (methanol). Yield: 52%; mp 140-142 °C; ^{1}H NMR ($CDCl_3$, 300.13 MHz): δ 7.76 (1H, d, J=15.5 Hz, H-β), 7.69 (1H, d, J=1.2 Hz, H-3'), 7.29 (1H, dd, J=1.3, 1.1 Hz, H-5'), 7.27 (1H, d, J =15.5 Hz, H-α), 6.86 (2H, s, H-2,-6), 3.93 (6H, s, 3-,5-OCH_3), 3.91 (3H, s, 4-OCH_3), 2.34 (3H, s, 4'-CH_3); ^{13}C NMR ($CDCl_3$ 75.47 MHz): δ 181.9 (C=O), 153.5 (C- 3,-5), 145.0 (C-2'), 144.0 (C-β), 140.5 (C-4), 139.0 (C-4'), 133.7 (C-3'), 130.7 (C-1), 129.8 (C-5'), 120.9 (C-α), 105.7 (C-2,-6), 61.0 (4-OCH_3), 56.3 (3-,5-OCH_3), 15.7 (4'-CH_3); ESI-HRMS (+) *m/z*: Anal. Calc. for $C_{17}H_{19}O_4S$ $(M+H)^+$: 319.09986; found: 319.09920.

*(E)-1-(4-methylthiophen-2-yl)-3-(2,4,5-trimethoxyphenyl)prop-2-en-1-one (**10**).* Purified by flash column chromatography (*n*-hexane: acetone, 7:3) followed by crystallization (methanol: chloroform). Yield: 23 %; mp: 107-109 ºC; ^{1}H NMR ($CDCl_3$ 300.13 MHz): δ 8.11 (1H, d, J=15.6 Hz, H-β), 7.65 (1H, d, J=1.2 Hz, H-3'), 7.35 (1H, d, J= 15.6 Hz, H-α), 7.24 (1H, dd, J= 1.3, 1.1 Hz, H-5'), 7.12 (1H, s, H-6), 6.53 (1H, s, H-3), 3.95 (3H, s, 2-OCH_3), 3.92 (3H, s, 4-OCH_3); 3.91 (3H, s, 5-OCH_3), 2.33 (3H, s, 4'-CH_3); ^{13}C NMR ($CDCl_3$, 75.47 MHz): δ 182.5 (C=O), 154.8 (C-2), 152.5 (C-4), 145.5 (C-2'), 143.2 (C-5), 139.2 (C-β), 138.9 (C-4'), 133.3 (C-3'), 129.0 (C-5'), 119.9 (C-α), 115.4

(C-1), 111.7 (C-6), 96.8 (C-3), 56.6 (4-OCH_3), 56.4 (5-OCH_3), 56.1 (2-OCH_3), 15.7 (4'-CH_3); ESI-HRMS (+) *m/z*: Anal. Calc. for $C_{17}H_{19}O_4S$ $(M+H)^+$: 319.09986; found: 319.09957.

*(E)-3-(3,5-dichlorophenyl)-1-(4-methylthiophen-2-yl)prop-2-en-1-one (**13**).* Purified by crystallization (methanol: chloroform). Yield: 65%; mp: 112-115 ºC; ^{1}H NMR ($CDCl_3$ 300.13 MHz): δ 7.69 (1H, d, J=1.2 Hz, H-3'), 7.67 (1H, d, J=15.7 Hz, H-β), 7.49 (2H, d, J=1.9 Hz, H-2,-6), 7.39 (1H, t, J=1.9 Hz, H-4), 7.37 (1H, d, J=15.7 Hz, H-α), 7.23 (1H, dd, J=1.3, 1.1 Hz, H-5'), 2.34 (3H, s, 4'-CH_3); ^{13}C NMR ($CDCl_3$, 75.47 MHz): δ 181.6 (C=O), 145.0 (C-2'), 141.0 (C-β), 139.7 (C-4'), 138.2 (C-1), 136.1 (C-3,-5), 134.7 (C-3'), 131.0 (C-5'), 130.4 (C-4), 126.9 (C-2,-6), 124.5 (C-α), 16.1 (4'-CH_3); ESI-HRMS (+) *m/z*: Anal. Calc. for $C_{14}H_{11}Cl_2OS$ $(M+H)^+$: 296.99022; found: 296.99025.

*(E)-3-(3,4-dichlorophenyl)-1-(4-methylthiophen-2-yl)prop-2-en-1-one (**14**).* Purified by crystallization (methanol: chloroform). Yield: 67%; mp: 120-122 ºC; ^{1}H NMR ($CDCl_3$ 300.13 MHz): δ 7.72 (1H,d, J=1.9 Hz, H-2), 7.70 (1H, d, J=15.6 Hz, H-β), 7.69 (1H, d, J=1.2 Hz, H-3'), 7.50 (1H, d, J=8.4 Hz, H-5), 7.45 (1H, dd, J=8.4, 1.9 Hz, H-6), 7.35 (1H, d, J=15.6 Hz, H-α), 7.31 (1H, dd, J=1.3, 1.1 Hz, H-5'), 2.33 (3H, s, 4'-CH_3); ^{13}C NMR ($CDCl_3$, 75.47 MHz): δ 181.4 (C=O), 144.6 (C-2'), 141.0 (C-β), 139.2 (C-4'), 134.8 (C-1), 134.4 (C-4), 134.2 (C-3'), 133.3 (C-3), 131.0 (C-5'), 130.4 (C-5), 129.7 (C-2), 127.6 (C-6), 123.2 (C-α), 15.7 (4'-CH_3); ESI-HRMS (+) *m/z*: Anal. Calc. for $C_{14}H_{11}Cl_2OS$ $(M+H)^+$: 296.99022; found: 296.99019.

*(E)-1-(5-methylthiophen-2-yl)-3-(3,4,5-trimethoxyphenyl)prop-2-en-1-one (**15**).* Purified by flash column chromatography (n-hexane: ethyl acetate, 7:3) followed by crystallization (methanol: chloroform). Yield: 16 %; mp: 126-128 ºC; ^{1}H NMR ($CDCl_3$ 300.13 MHz): δ 7.74 (1H, d, J=15.4 Hz, H-β), 7.70 (1H, d, J=3.5 Hz, H-3'), 7.26 (1H, d, J= 15.5 Hz, H-α), 6.87 (1H, d, J= 3.5 Hz, H-4'), 6.85 (2H, s, H-2,-6), 3.93 (6H, s, 3-, 5-OCH_3), 3.90 (3H, s, 4-OCH_3), 2.57 (3H, s, 5'-CH_3); ^{13}C NMR ($CDCl_3$, 75.47 MHz): δ 181.5 (C=O), 153.5 (C-3, -5), 150.1 (C-5'), 143.6 (C-2'), 143.4 (C-β), 140.3 (C-4), 132.4 (C-3'), 130.4 (C-1), 126.9 (C-4'), 120.8 (C-α), 105.6 (C-2,-6), 61.0 (4- OCH_3), 56.2 (3-,5- OCH_3), 16.2 (5'-CH_3); ESI-HRMS (+) *m/z*: Anal. Calc. for $C_{17}H_{19}O_4S$ $(M+H)^+$: 319.09986; found: 319.09904.

(E)-1-(benzo[b]thiophen-2-yl)-3-(3,4,5-trimethoxyphenyl)prop-2-en-1-one ***(16)***. Purified by flash column chromatography (n-hexane: ethyl acetate, 7:3) followed by crystallization (methanol: chloroform). Yield: 38 %; mp> 350ºC; ^{1}H NMR ($CDCl_3$, 300.13 MHz): δ 8.13 (1H, s, H-3'), 7.95-7.90 (2H, m, H-4,'-7'), 7.83 (1H, d, J=15.5 Hz, H-β), 7.58 (1H, d, J=15.5 Hz, H-α), 7.52-7.41 (2H, m, H-5',-6'), 6.91 (2H, s, H-2,-6), 3.96 (6H, s, 3-,5-OCH_3), 3.92 (3H, s, 4-OCH_3); ^{13}C NMR ($CDCl_3$ 75.47 MHz): δ 171.2 (C=O), 153.5 (C-3,-5), 145.2 (C-8'), 144.6 (C-β), 143.0 (C-2'), 140.7 (C-4), 139.3 (C-9'), 130.1 (C-1), 128.8 (C-3'), 127.4 (C-7'), 125.9 (C-4'), 125.1 (C-6'), 123.1 (C-5'), 120.4 (C-α), 105.8 (C-2,-6), 61.1 (4-OCH_3), 56.3 (3-,5-OCH_3); ESI-HRMS (+) *m/z*: Anal. Calc. for $C_{20}H_{19}O_4S$ $(M+H)^+$: 355.09986; found: 355.09935.

(E)-1-(7-hydroxybenzofuran-2-yl)-3-(3,4,5-trimethoxyphenyl)prop-2-en-1-one ***(17)***. Purified by flash column chromatography (n-hexane: ethyl acetate, 5:5) followed by flash column chromatography (n-hexane: ethyl acetate, 5:5). Yield: 12 %; mp: 190-192ºC; ^{1}H NMR ($CDCl_3$, 300.13 MHz): δ 7.89 (1H, d, J = 15.6 Hz, H-β), 7.68 (1H, s, H-3'), 7.43 (1H, d, J=15.6 Hz, H-α), 7.29 (1H, dd, J=7.8, 1.1 Hz, H-4'), 7.21 (3H, t, J=7.8 Hz, H-5'), 7.06 (1H, dd, J=7.7, 1.1 Hz, H-6'), 6.91 (2H, s, H-2,-6), 3.94 (6H, s, 3-,5-OCH_3), 3.92 (3H, s, 4-CH_3); ^{13}C NMR ($CDCl_3$ 75.47 MHz): δ 179.5 (C=O), 153.6 (C-2'), 153.5 (C-3,-5), 145.3 (C-β), 144.6 (C-8'), 141.8 (C-7'), 140.9 (C-4), 130.0 (C-1), 128.8 (C-9'), 125.9 (C-6'), 120.1 (C-α), 115.0 (C-4'), 114.2 (C-3',-5'), 106.1 (C-2,-6), 61.1 (4-OCH_3), 56.3 (3-,5-OCH_3); ESI-HRMS (+) *m/z*: Anal. Calc. for $C_{20}H_{19}O_6$ $(M+H)^+$: 355.11761; found: 355.11710.

Synthesis of epoxide derivatives **24** and **25**. To a solution of chalcones **3** (1.56 mmol, 0.5 g) or **9** (1.50 mmol, 0.5 g) in methanol or methanol:acetone (3:2, 30 mL) was added powdered K_2CO_3 (0.622 g, 4.5 mmol) or a solution of 5% NaOH (3.84 mL), respectively, followed by the dropwise addition of 30% hydrogen peroxide (0.96 mL, 8.5 mmol) at 0-4 ºC. The reaction mixture was stirred at room temperature for 2-3 h, and after was left in the dark overnight at -20 ºC. The obtained solid was filtered, and washed with water. The solid obtained was purified by crystallization (dichloromethane: methanol).

*Thiophen-2-yl(3-(3,4,5-trimethoxyphenyl)oxiran-2-yl)methanone (**24**)*. Yield: 61%; mp (dichloromethane : methanol): 111-113 ºC; ^{1}H NMR ($CDCl_3$, 300.13 MHz): δ 8.01 (1H, dd, J=3.9, 1.1 Hz, H-5'), 7.76 (1H, dd, J=4.9, 1.1 Hz, H-3'), 7.19 (1H, dd, J= 4.9, 3.9 Hz, H-4'), 6.57 (2H, s, H-2,-6), 4.13 (1H, d, J= 1.8 Hz, H-1''), 4.03 (1H, d, J= 1.8 Hz, H-2''), 3.87 (6H, s, 3, 5-OCH_3), 3.86 (3H, s, 4-OCH_3); ^{13}C NMR ($CDCl_3$, 75.47 MHz): δ 186.3 (C=O), 153.7 (C-3, -5), 140.9 (C-2'), 138.5 (C-4), 135.3 (C-3'), 133.7 (C-5'), 130.9 (C-1), 128.5 (C-4'), 102.5 (C-2, -6), 62.0 (C-2''), 60.9 (4-OCH_3), 59.7 (C-1''), 56.2 (3-,5-OCH_3); ESI-HRMS (+) *m/z*: Anal. Calc. for $C_{16}H_{16}NaO_5S$ $(M+Na)^+$: 343.06107; found: 343.06327.

*(4-methylthiophen-2-yl)(3-(3,4,5-trimethoxyphenyl)oxiran-2-yl)methanone (**25**)*. Yield: 58%; mp (dichloromethane: methanol): 104-108 ºC; ^{1}H NMR ($CDCl_3$, 300.13 MHz): δ 7.79 (1H, d, J=1.2 Hz, H-3'), 7.35 (1H, t, J= 1.2 Hz, H-5'), 6.56 (2H, s, H-2,-6), 4.12 (1H, d, J= 1.8, H-1''), 4.00 (1H, d, J= 1.8, H-2''), 3.87 (6H, s, 3-,5-OCH_3), 3.86 (3H, s, 4-OCH_3), 2.31 (1H,s, 4' -CH_3). ^{13}C NMR ($CDCl_3$, 75.47 MHz): δ= 186.2 (C=O), 153.7 (C-3,-5), 140.6 (C-2'), 139.4 (C-4, -4'), 135.4 (C-3'), 131.3 (C-1), 131.0 (C-5'), 102.4 (C-2,-6), 61.8 (C-2''), 60.9 (4-OCH_3), 59.6 (C-1''), 56.2 (3-,5-OCH_3), 15.5 (4'-CH_3); ESI-HRMS (+) *m/z*: Anal. Calc. for $C_{17}H_{19}0_5S$ $(M+Na)^+$: 357.07672; found: 357.07976.

Synthesis of pyrazole derivatives **26** and **27**. To a solution of epoxide derivatives **24** (0.9 mmol, 317 mg) or **25** (1.2 mmol, 387 mg) in xylenes (4-7 mL) and dichloromethane (2-4 mL) was added hydrazine hydrate (2.7-3.6 mmol) and *p*-toluenesulfonic acid monohydrate (0.11-0.15 mmol, 24.5-30.5 mg). The reaction mixture was stirred during 3-5 h at 100 ºC. After, the xylenes were removed under nitrogen stream and the solid obtained was purified as indicated below for the referred pyrazole derivatives.

*3-(thiophen-2-yl)-5-(3,4,5-trimethoxyphenyl)-1H-pyrazole (**26**)*. Purified by flash column chromatography (*n*-hexane: ethyl acetate, 6:4) followed by preparative TLC (*n*-hexane: ethyl acetate, 6:4). Yield: 4%; mp 70-72ºC; ^{1}H NMR ($CDCl_3$, 300.13 MHz): δ 7.36 (1H, d, J= 3.8 Hz, H-5'), 7.27 (1H, dd, J= 5.0, 3.6 Hz, H-3'), 7.03 (1H, d, J=5.0, 3.8 Hz, H-4'), 6.96 (2H, s, H-2,-6), 6.69 (1H, s, H-2''), 3.90 (6H, s, 3-,5-OCH_3), 3.88

(3H, s, 4-OCH_3); ^{13}C NMR ($CDCl_3$, 75.47 MHz) δ= 153.5 (C-3,-5), 147.5 (C-1''), 144.0 (C-2'), 138.8 (C-4), 134.0 (C-3''), 127.9 (C-3'), 126.0 (C-5'), 125.8 (C-1), 125.2 (C-4'), 103.3 (C-2, -6), 100.1 (C-2''), 61.0 (4 -OCH_3), 56.3 (3-, 5- OCH_3); ESI-HRMS (+) *m/z*: Anal. Calc. for $C_{16}H_{17}N_2O_3S$ $(M+H)^+$: 317.09544; found: 317.09495.

*3-(4-methylthiophen-2-yl)-5-(3,4,5-trimethoxyphenyl)-1H-pyrazole (***27***).* Purified by flash column chromatography (*n*-hexane: ethyl acetate, 6:4) followed by preparative TLC (*n*-hexane: ethyl acetate, 6:4). Yield: 1%; mp 84-86 ºC; ^1H NMR ($CDCl_3$, 500 MHz): δ 7.64 (1H, brs, H-5'), 7.13 (1H, brs, H-3'), 6.87 (1H, s, H-2''), 6.63 (2H, s, H-2,-6), 3.89 (6H, s, 3-,5-OCH_3), 3.80 (3H, s, 4-OCH_3), 2.22 (3H, s, 4'-CH_3); ^{13}C NMR ($CDCl_3$, 120 MHz) δ= 153.2 (C-3,-5), 143.1 (C-1''), 137.9 (C-2'), 137.2 (C-4), 133.7 (C-3''), 128.5 (C-4'), 128.0 (C-3'), 125.1 (C-5'), 121.2 (C-1), 109.3 (C-2''), 106.1 (C-2, -6), 61.0 (4 -OCH_3), 56.1 (3-,5- OCH_3), 15.7 (4'-CH_3); ESI-HRMS (+) *m/z*: Anal. Calc. for $C_{17}H_{19}N_2O_3S$ $(M+H)^+$: 331.11109; found: 331.11060.

3.3. Growth Inhibitory effect in Human Tumor Cell Lines

Cell Culture. The human tumor cell lines melanoma A375-C5, breast adenocarcinoma MCF-7, and non-small cell lung cancer NCI-H460 (European Collection of Cell Culture, UK) were grown in RPMI-1640 culture medium (Lonza, Basel, Switzerland), supplemented with 5% fetal bovine serum (FBS), and cells were maintained at 37 °C in a 5% CO_2 humidified atmosphere.

Compound preparation. All compounds were dissolved in sterile DMSO at 60 mM stock, with the exception **26** which was dissolved at 10 mM. Nocodazole and paclitaxel (Sigma-Aldrich Co., Saint Louis, MO, USA) were dissolved in DMSO as 0.5 mM stock. To avoid repeated freeze-thaw cycles, the 60 or 10 mM of stock solution were stored in different aliquots, at -20 ºC. Appropriate dilutions of the compounds were freshly diluted in RPMI medium culture.

Viability assays. Cells were plated in 96-well plates at 0.05×10^6 cells/well in complete medium at 37 °C for twenty-four h. Then, two-fold serial dilutions of the test compounds were added to culture medium, at concentrations ranging from 0 to 150 µM,

for 48 h. Control groups were treated with equivalent amount, up to 0.25% concentration, of the solvent dimethyl sulfoxide (DMSO, Sigma-Aldrich). Then, cells were fixed with 50% (m/v) trichloroacetic acid (Merck Millipore, Darmstadt, Germany), washed with distilled water and stained with sulforhodamine B (SRB; Sigma-Aldrich) for 30 min at room temperature. After a 5 times wash with 1% (v/v) acetic acid (Merck Millipore), plates were left to dry at room temperature before SRB complexes solubilization with 10 mM Tris buffer (Sigma-Aldrich) for 30 min. Cell survival was measured through determination of the absorbance at 515 nm in a microplate reader (Biotek Synergy 2, BioTek Instruments, Inc., Winooski, VT, USA). The 50% cell growth inhibition concentration (GI_{50}) was calculated using the dose–response curve established for each test compound.

Alternatively, for combination experiments with paclitaxel, cell viability was assessed by MTT assay. Cells were plated in 96-well plates (0.05×10^6 cells/well) in complete culture medium and incubated at 37 °C for 24 h. Cells were then incubated for 48 h with the test compound, paclitaxel, or a combination of both at 37 °C and 5% CO_2. Then, cells were placed in fresh serum-free medium, and 3-(4,5-dimethylthiazol-2-yl)-2,5-diphenyltetrazolium bromide (MTT), previously dissolved in PBS, was added to each well (0.5 mg/ml) and incubated for 4 h at 37 °C and 5% CO_2. Formazan crystals were then solubilized by adding 100 µL solubilization solution (89% Isopropanol, 10% of Triton-100, 0.37% HCl) for 2 h. Absorbance was measured at 570 nm in a microplate reader (Biotek Synergy 2), and retrieved through the Gene5 software (Biotek). Viability was calculated relative to untreated cells.

Determination of antimitotic activity. NCI-H460 cells (2×10^5) were grown in six-well dishes and treated for 24 h with the test compounds. Treatment with 1 µM nocodazole served as a positive control. Controls included untreated cells and cells treated with the highest concentration of DMSO used to dissolve the compounds. Mitotic index, percentage of mitotic cells over total cell population, was determined by cell-rounding under phase-contrast microscopy. For each condition, a total of 2000 mitotic and interphasic cells were counted from more than ten random microscope fields.

Indirect Immunofluorescence. A total of $0.15x10^6$ cells / well NCI-H460 cells were grown on poly-L-lysine coated coverslips, in six-well dishes, and were treated with the test compounds during 15 h. The respective controls were included as described for mitotic index determination. Cells were fixed with 2% paraformaldehyde (Sigma-Aldrich) in PBS for 12 min, and washed 3 times with PBS for 5 min. Cells were then permeabilized in 0.5% Triton X-100 in PBS for 7 min, and washed 3 times with PBS, for 5 min each. To avoid unspecific binding of the primary antibody, cells were treated with a blocking solution, consisting of 10% FBS in PBST (PBS plus 0.5% Tween 20), for 30 min, followed by an 1 h incubation with the primary antibody, mouse anti-α-Tubulin (Sigma-Aldrich) diluted at 1:2500 in PBST containing 5% FBS. After rinsing in PBST, cells were incubated for an extra 1 h with the Alexa Fluor 488 (Molecular Probes) conjugated secondary antibody diluted at 1:1500 in PBST with 5% FBS. DNA was stained with 2 µg/mL 4′, 6-diamidino-98 2-phenylindole (DAPI, Sigma-Aldrich) diluted in Vectashield mounting medium (Vector, H-1000).

Image acquisition and processing. Phase-contrast microscopy images were recorded with a 10x objective, on a Nikon TE 2000-U microscope (Amsterdam, Netherlands), using a DXM1200F digital camera (Amsterdam, Netherlands) and with Nikon ACT-1 software (version 2.62, Melville, NY, USA). Fluorescence images were acquired with Plan Apochromatic 63x/NA 1.4 objective or with 40x objective on an Axio Observer Z.1 SD microscope (Carl Zeiss, Germany), coupled to an AxioCam MR3. Z-stacks were acquired with 0.4 µm intervals and, after image deconvolution with AxioVision Release SPC software (version 4.8.2, Carl Zeiss, Germany), they were processed using ImageJ (version 1.44, Rasband, W.S., ImageJ, U. S. National Institutes of Health, Bethesda, MD, USA).

Statistical analysis. Statistical analysis was performed using an Unpaired Student t-test, or two-way ANOVA, in GraphPad Prism version 6 (GraphPad software Inc., CA, USA). Alpha value was 0.05 and the confidence interval 95%. Data are presented as the means ± standard deviation (SD) of at least three independent experiments, and was considered statistically significant when $p<0.05$.

3.4. Lipophilicity evaluation

Preparation of Liposomes. Liposomes were prepared based on the thin film hydration method [63]. A DMPC solution in chloroform:methanol (3:2) was dried at 40 °C under a nitrogen stream. The lipid film was then dispersed in HEPES buffer, vortexed, and extruded at 40 °C through polycarbonate filters. The extrusion was performed using the Lipex® extruder of Northern Lipids Inc. (Burnaby, Canada), and the filters were acquired from Whatman (Maidstone, UK).

General procedure for calibration curves. From the stock solution, $4X10^{-2}$ L mol^{-1}, prepared by dissolution of compound in DMSO, intermediate solutions were prepared within a range $6x10^{-4}$ to $1x10^{-2}$ L mol^{-1}. These solutions were further diluted with HEPES buffer yielding the final range of concentration between $6x10^{-5}$ to $1x10^{-3}$ L mol^{-1} (DMSO final percentage: 1%). Absorption spectra were recorded at 37 °C from 250 to 500 nm.

Determination of partition coefficients by derivative spectrophotometry. The procedure used for partition coefficient determination was adapted from the literature [64]. Briefly, to fixed concentration of the compound, previously defined by the calibration curve, increasing concentrations of DMPC (50-1000 µM) were added. Then, all suspensions were mixed and incubated for 30 min at 37 °C. The correspondent reference suspensions were identically prepared without compound. The absorption spectra (250–500 nm range) of the samples and respective reference solutions were recorded at 37 °C.

The mathematical treatment of the obtained spectra was performed using a previously reported routine [64]. Partition coefficient (K_P) was calculated by fitting the second derivative spectra values, at wavelengths where the scattering is eliminated, in function of liposome concentration, following Equation 1:

(1)

where D is the second derivative of absorbance: D_T refers to the absorbance of the total amount of compound in a sample suspension, D_b and D_m correspond to the compound absorbance when distributed in the buffer and in the liposome phase, respectively. K_p is the partition coefficient, [L] is the lipid molar concentration and V_Φ is the lipid molar volume, which is 0.66 L mol^{-1} [65]. Fitting experimental data to Equation 1 was

conducted through a non-linear least-squares regression method with Origin 2017 (Originlab Corporation, Washington, DC, USA). Log K_p values are expressed as dimensionless and presented as means ± SD from at least three independent experiments.

4. Conclusions

In this work, twenty-four chalcone derivatives, including epoxide and pyrazole derivatives, with features compatible with a good oral bioavailability were synthetized and evaluated for their antiproliferative activity in human tumor cell lines. Among these, methoxylated chalcones **3**, **5**, **9**, **11**, **15-19**, and **22** demonstrated a potent antiproliferative activity in the three human tumor cell lines studied, being this effect associated with an antimitotic effect. Mechanistically, compounds **15-17** emerged as potent antimitotic agents by interfering with mitotic spindle assembly, ultimately leading to cell death. Interestingly, compound **15** sensitizes human tumor cells to death by low doses of paclitaxel, which might provide therapeutic benefits by overcoming problems of resistance and side effects. The analysis of lipophilicity and antiproliferative activity of these compounds suggests that a proper balance between hydrophilicity and lipophilicity, found for compounds with log K_P around 3.5, is necessary to achieve potent chalcone derivatives. In light of the aforementioned results, the present study contributes to open new routes in the area of research on new antitumor agents.

5. Acknowledgments

This research was partially supported by the Strategic Funding UID/Multi/04423/2019 through national funds provided by FCT (Foundation for Science and Technology) and European Regional Development Fund (ERDF), in the framework of the program PT2020, the projects PTDC/SAU-PUB/28736/2017 (reference POCI-01-0145-FEDER-028736), PTDC/MAR-BIO/4694/2014 (reference POCI-01-0145-FEDER-016790; Project 3599–PPCDT). This work was partially supported through funds provided by CESPU, Crl under the project ComeTarget_CESPU_2017. Ana Henriques and Joana

Moreira acknowledge for their FCT grants (SFRH/BD/111365/2015 and SFRH/BD/135852/2018, respectively). José Soares thanks FCT (Fundação para a Ciência e Tecnologia) and POPH (Programa Operacional Potencial Humano) for his Ph.D. grant Ref. SFRH/BD/98105/2013, and also the Biotech Health Programme (Doctoral Programme on Cellular and Molecular Biotechnology Applied to Health Sciences), Reference PD/00016/2012. The authors thank Sara Cravo for all the technic and scientific support.

6. References

[1] B. van der Vaart, A. Akhmanova, A. Straube, Regulation of microtubule dynamic instability, Biochem. Soc. Trans. 37 (2009) 1007–1013. https://doi.org/10.1042/BST0371007

[2] M.A. Jordan, L. Wilson, Microtubules as a target for anticancer drugs, Nat. Rev. Cancer. 4 (2004) 253-265. https://doi.org/10.1038/nrc1317

[3] E.A. Perez, Microtubule inhibitors: Differentiating tubulin-inhibiting agents based on mechanisms of action, clinical activity, and resistance, Mol. Cancer Ther. 8 (2009) 2086-2095. https://doi.org/10.1158/1535-7163

[4] M. Kavallaris, Microtubules and resistance to tubulin-binding agents, Nat. Rev. Cancer. 10 (2010) 194-204. https://doi.org/10.1038/nrc2803

[5] E. Mukhtar, V.M. Adhami, H. Mukhtar, Targeting microtubules by natural agents for cancer therapy, Mol. Cancer Ther. 13 (2014) 275-284. https://doi.org/10.1158/1535-7163

[6] P. Singh, A. Anand, V. Kumar, Recent developments in biological activities of chalcones: A mini review, Eur. J. Med. Chem. 85 (2014) 758-777. https://doi.org/10.1016/j.ejmech.2014.08.033

[7] W.-Y. Fang, L. Ravindar, K. Rakesh, H. Manukumar, C. Shantharam, N.S. Alharbi, H.-L. Qin, Synthetic approaches and pharmaceutical applications of chloro-containing molecules for drug discovery: A critical review, Eur. J. Med. Chem. (2019) 117-153. https://doi.org/10.1016/j.ejmech.2019.03.063

[8] C. Zhao, K. Rakesh, L. Ravidar, W.-Y. Fang, H.-L. Qin, Pharmaceutical and medicinal significance of sulfur (SVI)-containing motifs for drug discovery: A critical

review, Eur. J. Med. Chem. (2018) 679-734. https://doi.org/10.1016/j.ejmech.2018.11.017

[9] M. Xu, P. Wu, F. Shen, J. Ji, K. Rakesh, Chalcone derivatives and their antibacterial activities: Current development, Bioorg. Chem. 91 (2019) 103133. https://doi.org/10.1016/j.bioorg.2019.103133

[10] X. Zhang, K. Rakesh, S. Bukhari, M. Balakrishna, H. Manukumar, H.-L. Qin, Multi-targetable chalcone analogs to treat deadly Alzheimer's disease: Current view and upcoming advice, Bioorg. Chem. 80 (2018) 86-93. https://doi.org/10.1016/j.bioorg.2018.06.009

[11] C. Zhuang, W. Zhang, C. Sheng, W. Zhang, C. Xing, Z. Miao, Chalcone: a privileged structure in medicinal chemistry, Chem. Rev. 117 (2017) 7762-7810. https://doi.org/10.1021/acs.chemrev.7b00020

[12] H. Albuquerque, C. Santos, J. Cavaleiro, A. Silva, Chalcones as Versatile Synthons for the Synthesis of 5-and 6-membered Nitrogen Heterocycles, Curr. Org. Chem. 18 (2014) 2750-2775. https://doi.org/10.2174/1385272819666141013224253

[13] S. Ducki, Antimitotic chalcones and related compounds as inhibitors of tubulin assembly, Anti-cancer agent. Me. 9 (2009) 336-347. https://doi.org/10.2174/1871520610909030336

[14] M.P. Neves, R.T. Lima, K. Choosang, P. Pakkong, M.S.J. Nascimento, M.H. Vasconcelos, M. Pinto, A.M. Silva, H. Cidade, Synthesis of a Natural Chalcone and Its Prenyl Analogs–Evaluation of Tumor Cell Growth□Inhibitory Activities, and Effects on Cell Cycle and Apoptosis, Chem. Biodivers. 9 (2012) 1133-1143. https://doi.org/10.1002/cbdv.201100190

[15] M.P. Neves, S. Cravo, R.T. Lima, M.H. Vasconcelos, M.S.J. Nascimento, A.M. Silva, M. Pinto, H. Cidade, A.G. Corrêa, Solid-phase synthesis of 2′-hydroxychalcones. Effects on cell growth inhibition, cell cycle and apoptosis of human tumor cell lines, Biorg. Med. Chem. 20 (2012) 25-33. https://doi.org/10.1016/j.bmc.2011.11.042

[16] D. Pereira, R.T. Lima, A. Palmeira, H. Seca, J. Soares, S. Gomes, L. Raimundo, C. Maciel, M. Pinto, E. Sousa, Design and synthesis of new inhibitors of p53–MDM2 interaction with a chalcone scaffold, Arab. J. Chem. (2016) https://doi.org/10.1016/j.arabjc.2016.04.015

[17] P. Brandão, J.B. Loureiro, S. Carvalho, M.H. Hamadou, S. Cravo, J. Moreira, D. Pereira, A. Palmeira, M. Pinto, L. Saraiva, Targeting the MDM2-p53 protein-protein interaction with prenylchalcones: Synthesis of a small library and evaluation of potential antitumor activity, Eur. J. Med. Chem. 156 (2018) 711-721. https://doi.org/10.1016/j.ejmech.2018.07.037

[18] M. Leão, J. Soares, S. Gomes, L. Raimundo, H. Ramos, C. Bessa, G. Queiroz, S. Domingos, M. Pinto, A. Inga, Enhanced cytotoxicity of prenylated chalcone against tumour cells via disruption of the p53–MDM2 interaction, Life Sci. 142 (2015) 60-65. https://doi.org/10.1016/j.lfs.2015.10.015

[19] K. Masawang, M. Pedro, H. Cidade, R.M. Reis, M.P. Neves, A.G. Corrêa, W. Sudprasert, H. Bousbaa, M.M. Pinto, Evaluation of 2′, 4′-dihydroxy-3, 4, 5-trimethoxychalcone as antimitotic agent that induces mitotic catastrophe in MCF-7 breast cancer cells, Toxicol. Lett. 229 (2014) 393-401. https://doi.org/10.1016/j.toxlet.2014.06.016

[20] J. Fonseca, S. Marques, P. Silva, P. Brandão, H. Cidade, M. Pinto, H. Bousbaa, Prenylated chalcone 2 acts as an antimitotic agent and enhances the chemosensitivity of tumor cells to paclitaxel, Molecule. 21 (2016) 982. https://doi.org/10.3390/molecules21080982

[21] P.D. Leeson, B. Springthorpe, The influence of drug-like concepts on decision-making in medicinal chemistry, Nat. Rev. Drug Discov. 6 (2007) 881-890. https://doi.org/10.1038/nrd2445

[22] L. Di, E.H. Kerns, G.T. Carter, Drug-like property concepts in pharmaceutical design, Curr. Pharm. Des. 15 (2009) 2184-2194. https://doi.org/10.2174/138161209788682479

[23] W.P. Walters, M.A. Murcko, Prediction of 'drug-likeness', Adv. Drug Deliver Rev. 54 (2002) 255-271. https://doi.org/10.1016/S0169-409X(02)00003-0

[24] C.A. Lipinski, F. Lombardo, B.W. Dominy, P.J. Feeney, Experimental and computational approaches to estimate solubility and permeability in drug discovery and development settings, Adv. Drug Deliver Rev. 23 (1997) 3-25. https://doi.org/10.1016/S0169-409X(96)00423-1

[25] A.K. Ghose, V.N. Viswanadhan, J.J. Wendoloski, A knowledge-based approach in designing combinatorial or medicinal chemistry libraries for drug discovery. 1. A

805 qualitative and quantitative characterization of known drug databases, J. Comb. Chem.
806 1 (1999) 55-68. https://doi.org/10.1021/cc9800071
807 [26] D.F. Veber, S.R. Johnson, H.-Y. Cheng, B.R. Smith, K.W. Ward, K.D. Kopple,
808 Molecular properties that influence the oral bioavailability of drug candidates, J. Med.
809 Chem. 45 (2002) 2615-2623. https://doi.org/10.1021/jm020017n
810 [27] W.J. Egan, K.M. Merz, J.J. Baldwin, Prediction of drug absorption using
811 multivariate statistics, J. Med. Chem. 43 (2000) 3867-3877.
812 https://doi.org/10.1021/jm000292e
813 [28] T.I. Oprea, Property distribution of drug-related chemical databases*, J. Comput.
814 Aided Mol. Des. 14 (2000) 251-264. https://doi.org/10.1023/a:1008130001697
815 [29] I. Muegge, S.L. Heald, D. Brittelli, Simple selection criteria for drug-like chemical
816 matter, J. Med. Chem. 44 (2001) 1841-1846. https://doi.org/10.1021/jm015507e
817 [30] R.D. Brown, M. Hassan, M. Waldman, Tools for designing diverse, druglike, cost-
818 effective combinatorial libraries, in: Combinatorial Library Design and Evaluation,
819 CRC Press, 2001, pp. 321-356.
820 [31] X. Liu, B. Testa, A. Fahr, Lipophilicity and its relationship with passive drug
821 permeation, Pharm. Res. 28 (2011) 962-977. https://doi.org/10.1007/s11095-010-0303-
822 7
823 [32] L. Feng, R.J. Mumper, A critical review of lipid-based nanoparticles for taxane
824 delivery, Cancer lett. 334 (2013) 157-175. https://doi.org/10.1016/j.canlet.2012.07.006
825 [33] C.D. Scripture, W.D. Figg, A. Sparreboom, Peripheral neuropathy induced by
826 paclitaxel: recent insights and future perspectives, Curr. Neuropharmacol. 4 (2006) 165-
827 172. https://doi.org/10.2174/157015906776359568
828 [34] Á. Santos, J.X. Soares, S. Cravo, M.E. Tiritan, S. Reis, C. Afonso, C. Fernandes,
829 M.M. Pinto, Lipophilicity assessement in drug discovery: Experimental and theoretical
830 methods applied to xanthone derivatives, J. Chromatogr. B 1072 (2018) 182-192.
831 https://doi.org/10.1016/j.jchromb.2017.10.018
832 [35] M. Lucio, J. Lima, S. Reis, Drug-membrane interactions: significance for
833 medicinal chemistry, Curr. Med. Chem. 17 (2010) 1795-1809.
834 https://doi.org/10.2174/092986710791111233
835 [36] C.M. Azevedo, C.M. Afonso, J.X. Soares, S. Reis, D. Sousa, R.T. Lima, M.H.
836 Vasconcelos, M. Pedro, J. Barbosa, L. Gales, Pyranoxanthones: Synthesis, growth

inhibitory activity on human tumor cell lines and determination of their lipophilicity in two membrane models, Eur. J. Med. Chem. 69 (2013) 798-816. https://doi.org/10.1016/j.ejmech.2013.09.012

[37] C. Pereira-Leite, C. Carneiro, J.X. Soares, C. Afonso, C. Nunes, M. Lúcio, S. Reis, Biophysical characterization of the drug–membrane interactions: the case of propranolol and acebutolol, Eur. J. Pharm. Biopharm. 84 (2013) 183-191. https://doi.org/10.1016/j.ejpb.2012.12.005

[38] D.R. Loureiro, J.X. Soares, D. Lopes, T. Macedo, D. Yordanova, S. Jakobtorweihen, C. Nunes, S. Reis, M.M. Pinto, C.M. Afonso, Accessing lipophilicity of drugs with biomimetic models: A comparative study using liposomes and micelles, Eur. J. Pharm. Sci. 115 (2018) 369-380. https://doi.org/10.1016/j.ejps.2018.01.029

[39] P. Lagisetty, P. Vilekar, K. Sahoo, S. Anant, V. Awasthi, CLEFMA—An anti-proliferative curcuminoid from structure–activity relationship studies on 3, 5-bis (benzylidene)-4-piperidones, Biorg. Med. Chem. 18 (2010) 6109-6120. https://doi.org/10.1016/j.bmc.2010.06.055

[40] B. Bhat, K. Dhar, S. Puri, A. Saxena, M. Shanmugavel, G. Qazi, Synthesis and biological evaluation of chalcones and their derived pyrazoles as potential cytotoxic agents, Biorg. Med. Chem. Lett. 15 (2005) 3177-3180. https://doi.org/10.1016/j.bmcl.2005.03.121

[41] E. Logarinho, H. Bousbaa, Kinetochore-microtubule interactions “in check” by Bub1, Bub3 and BubR1: The dual task of attaching and signalling, Cell cycle. 7 (2008) 1763-1768. https://doi.org/10.4161/cc.7.12.6180

[42] N.C. Santos, M. Prieto, M.A. Castanho, Quantifying molecular partition into model systems of biomembranes: an emphasis on optical spectroscopic methods, BBA-Biomembranes. 1612 (2003) 123-135. https://doi.org/10.1016/S0005-2736(03)00112-3

[43] H. Ferreira, M. Lúcio, J.L. Lima, C. Matos, S. Reis, Interaction of clonixin with EPC liposomes used as membrane models, J. Pharm. Sci. 94 (2005) 1277-1287. https://doi.org/10.1002/jps.20351

[44] H. Ferreira, M. Lúcio, B. de Castro, P. Gameiro, J.L. Lima, S. Reis, Partition and location of nimesulide in EPC liposomes: a spectrophotometric and fluorescence study, Anal. Bioanal. Chem. 377 (2003) 293-298. https://doi.org/10.1007/s00216-003-2089-5

[45] A. Daina, O. Michielin, V. Zoete, SwissADME: a free web tool to evaluate pharmacokinetics, drug-likeness and medicinal chemistry friendliness of small molecules, Sci. Rep. 7 (2017) 42717. https://doi.org/10.1038/srep42717

[46] S. Kogiso, S. Hosozawa, K. Wada, K. Munakata, Daphneolone in roots of Daphne odora, Phytochemistry. 13 (1974) 2332-2334. https://doi.org/10.1016/0031-9422(74)85059-4

[47] D.E. Pires, T.L. Blundell, D.B. Ascher, pkCSM: predicting small-molecule pharmacokinetic and toxicity properties using graph-based signatures, J. Med. Chem. 58 (2015) 4066-4072. https://doi.org/10.1021/acs.jmedchem.5b00104

[48] A. Lusci, G. Pollastri, P. Baldi, Deep architectures and deep learning in chemoinformatics: the prediction of aqueous solubility for drug-like molecules, J. Chem. Inf. Model. 53 (2013) 1563-1575. https://doi.org/10.1021/ci400187y

[49] VCCLAB, Virtual Computational Chemistry Laboratory. http://www.vcclab.org, 2005 (acceced 1 March 2018)

[50] H. Ohori, H. Yamakoshi, M. Tomizawa, M. Shibuya, Y. Kakudo, A. Takahashi, S. Takahashi, S. Kato, T. Suzuki, C. Ishioka, Synthesis and biological analysis of new curcumin analogues bearing an enhanced potential for the medicinal treatment of cancer, Mol. Cancer Ther. 5 (2006) 2563-2571. https://doi.org/10.1158/1535-7163

[51] J.B. Bertoldo, L.D. Chiaradia-Delatorre, A. Mascarello, P.C. Leal, M.N.S. Cordeiro, R.J. Nunes, E.S. Sarduy, P.J. Rosenthal, H. Terenzi, Synthetic compounds from an in house library as inhibitors of falcipain-2 from Plasmodium falciparum, J. Enzyme Inhib. Med. Chem. 30 (2015) 299-307. https://doi.org/10.3109/14756366.2014.920839

[52] V. Peyrot, D. Leynadier, M. Sarrazin, C. Briand, M. Menendez, J. Laynez, J.M. Andreu, Mechanism of binding of the new antimitotic drug MDL 27048 to the colchicine site of tubulin: equilibrium studies, Biochem. 31 (1992) 11125-11132. https://doi.org/10.1021/bi00160a024

[53] K.-J. Hwang, H.-S. Kim, I.-C. Han, B.-T. Kim, Synthesis of heterocyclic chalcone derivatives and their radical scavenging ability toward 2, 2-diphenyl-1-picrylhydrazyl (DPPH) free radicals, Bull. Korean Chem. Soc. 33 (2012) 2585-2591. https://doi.org/10.5012/bkcs.2012.33.8.2585

[54] S. Bag, S. Ramar, M.S. Degani, Synthesis and biological evaluation of α, β-unsaturated ketone as potential antifungal agents, Med. Chem. Res. 18 (2009) 309-316. https://doi.org/10.1007/s00044-008-9128-x

[55] F.B. Abdel, M.A. Khanfar, A.Y. Elnagar, F.A. Badria, A.M. Zaghloul, K.F. Ahmad, P.W. Sylvester, K.S. El, Design and pharmacophore modeling of biaryl methyl eugenol analogs as breast cancer invasion inhibitors, Biorg. Med. Chem. 18 (2010) 496-507. https://doi.org/10.1016/j.bmc.2009.12.019

[56] H.P. Ávila, E.d.F.A. Smânia, F. Delle Monache, A.S. Júnior, Structure–activity relationship of antibacterial chalcones, Biorg. Med. Chem. 16 (2008) 9790-9794. https://doi.org/10.1016/j.bmc.2008.09.064

[57] K. Juvale, V.F. Pape, M. Wiese, Investigation of chalcones and benzochalcones as inhibitors of breast cancer resistance protein, Biorg. Med. Chem. 20 (2012) 346-355. https://doi.org/10.1016/j.bmc.2011.10.074

[58] F.E. Cohen, J.H. McKerrow, C.S. Ring, P.J. Rosenthal, G.L. Kenyon, Z. Li, Inhibitors of metazoan parasite proteases, in, Google Patents, 1997.

[59] R. Kumar, P. Sharma, A. Shard, D.K. Tewary, G. Nadda, A.K. Sinha, Chalcones as promising pesticidal agents against diamondback moth (Plutella xylostella): microwave-assisted synthesis and structure–activity relationship, Med. Chem. Res. 21 (2012) 922-931. https://doi.org/10.1007/s00044-011-9602-8

[60] C.W. Mai, M. Yaeghoobi, N. Abd-Rahman, Y.B. Kang, M.R. Pichika, Chalcones with electron-withdrawing and electron-donating substituents: anticancer activity against TRAIL resistant cancer cells, structure–activity relationship analysis and regulation of apoptotic proteins, Eur. J. Med. Chem. 77 (2014) 378-387. https://doi.org/10.1016/j.ejmech.2014.03.002

[61] J. Wu, C. Wang, Y. Cai, J. Peng, D. Liang, Y. Zhao, S. Yang, X. Li, X. Wu, G. Liang, Synthesis and crystal structure of chalcones as well as on cytotoxicity and antibacterial properties, Med. Chem. Res. 21 (2012) 444-452. https://doi.org/10.1007/s00044-011-9549-9

[62] S. Khatib, O. Nerya, R. Musa, M. Shmuel, S. Tamir, J. Vaya, Chalcones as potent tyrosinase inhibitors: the importance of a 2, 4-substituted resorcinol moiety, Biorg. Med. Chem. 13 (2005) 433-441. https://doi.org/10.1016/j.bmc.2004.10.010

930 [63] H. Zhang, Thin-Film Hydration Followed by Extrusion Method for Liposome
931 Preparation, in: G.G.M. D'Souza (Ed.) Liposomes, Humana Press 2017, pp. 17-22.
932 [64] L.M. Magalhães, C. Nunes, M. Lúcio, M.A. Segundo, S. Reis, J.L.F.C. Lima,
933 High-throughput microplate assay for the determination of drug partition coefficients,
934 Nature Protocols. 5 (2010) 1823-1830. https://doi.org/10.1038/nprot.2010.137
935 [65] A.R. Neves, C. Nunes, H. Amenitsch, S. Reis, Effects of resveratrol on the
936 structure and fluidity of lipid bilayers: a membrane biophysical study, Soft matter. 12
937 (2016) 2118-2126. https://doi.org/10.1039/C5SM02905H

938

Highlights

- Chalcones **3**, **5**, **9**, **11**, and **15-19** displayed potent antiproliferative activity in tumor cell lines.
- The antimitotic effect of chalcones **15-17** was investigated.
- **15** was able to enhance chemosensitivity of tumor cells to paclitaxel.
- Lipophilicity was determined and a structure-property relationship was proposed.
- **3**, **5**, **9**, **11**, and **15-19** showed suitable drug-like lipophilicity.